

A non linear Full-FEM 3D model to describe pile-soil interaction under static and cyclic loading conditions

By

Michail Korres

In Partial Fulfillment of the Requirements for the Degree of

Master of Research

"Multiscale Approaches for Materials and Structures"

École Nationale des Ponts et Chaussées
2017 - 2018

Committee in charge:

Stefano Cherubini, EDF R&D
Vinicius Alves Fernandes, EDF R&D
Prof. Luc Dormieux, ENPC
Asst. Prof. Achilleas Papadimitriou, NTUA

Acknowledgements

First of all I would like to thank my supervisors, Stefano Cherubini and Vinicius Alves Fernandes, for the opportunity to participate in this internship and work with them. Their availability and motivation as well as their useful advices and support in and out of the scope of this internship's "subject", helped in the fulfillment of the present work. It was a great pleasure having shared my thoughts and difficulties with you.

I would also like to thank all my colleagues at EDF R&D for the warm welcome and the amazing ambiance that created. It is for your approachable and friendly behavior that I had the opportunity to feel like a part of this group.

Finally, I would like to thank my family for always being by my side, either physically or mentally. To my brother Thanasis and my parents Eliza and Stratos, without whom I wouldn't be able to advance until this point.

To Ioanna, for your support all over those years, for your love and patience, thank you for everything.

Abstract

Deep foundations consist of a practical solutions when specific geotechnical constraints do not allow the use of shallow foundations for the support of the superstructure. Pile-soil interaction remains a complex problem strongly influenced by non-linear phenomena of unilateral friction of the interface, as well as soil behavior. Standard design methods are based on approximations and correlations with experimental results while the estimation of soil's mechanical properties consists from it's own quite an uncertain task. On this context, numerical analysis can be of important support for the design and analysis of geotechnical structures.

A full-FEM 3D model with code_aster is proposed for a soil-pile geotechnical structure. Interface behavior is modeled with the use of joint elements where Coulomb's friction law control sliding. Non-linear behavior of soil is considered in an elasto-plastic framework adopting different soil modeling hypothesis. The proposed model is tested under different loading conditions axial/lateral, monotone or cyclic, and sensibility studies are examined so as to identify the impact of important parameters. A comparison with experimental results provides the validation of the proposed modeling strategy/strategies.

Keywords : pile-soil interaction, 3D Full-FEM model, joint elements, elastoplastic constitutive model, cyclic loading

Resumé

Les fondations profondes sont des solutions pratiques quand l'utilisation des fondations superficielles n'est pas autorisée à cause de limitations géotechniques du site d'intérêt. L'interaction sol-pieu reste un problème complexe fortement influencé par le comportement non-linéaire du frottement de l'interface, ainsi que du sol autour et à la pointe du pieu. Les méthodes de dimensionnement sont actuellement basées sur des approximations et corrélations avec des résultats expérimentaux, quand l'estimation des caractéristiques mécaniques est aussi une source d'incertitude très importante. Dans ce cadre, les approches numériques fournissent un outil très important quand à l'analyse et dimensionnement des ouvrages géotechniques.

Un modèle 3D Full-FEM avec code_aster est proposé pour une structure géotechnique pieu-sol. Le comportement de l'interface est modélisé avec des éléments joints où la loi de frottement de Coulomb gère le glissement de l'interface. Un comportement non-linéaire pour le sol, développé dans un contexte élasto-plastique, admet différentes hypothèses pour le comportement du sol. Le modèle en question est testé sous différents types de chargement : axiale/latéral, monotone ou cyclique. Des études de sensibilité ont été réalisés afin d'identifier l'impact des paramètres du modèle au comportement global du système. Une comparaison avec de résultats expérimentaux fournit la validation de la stratégie de modélisation proposée.

Mots clès : Interaction pieu-sol, modèle 3D full-FEM, éléments joints, comportement elastoplastique, chargement cyclique

Contents

List of Tables

List of Figures

1 Introduction

1.1 Background and Motivation

Deep foundations consist of a technical solution that can be applied in numerous cases where geotechnical constraints do not allow the use of typical shallow foundations. This is the case for example for the construction of new nuclear installations constructed by EDF.

In France, design standards consider only shallow foundations for nuclear structures. Following the Fukushima accident and after the requirement of the french Nuclear Safety Authority (Arrêté démonstration de sûreté dit "INB" - 7/2/2012), EDF has to justify and increase the safety of the existing and future nuclear power plants. In the framework of the post-Fukushima, new facilities called "Noyau Dur" have been designed or reinforced in order to withstand extreme events beyond sizing. Limited emplacements are available for new structures to be added on sites (as post-Fukushima requirements), and the criteria for the design of shallow foundations cannot always be met for these emplacements due to existing geotechnical constraints. Therefore, deep foundations as well as soil reinforcement by rigid inclusions have to be examined.

Pile-soil interaction has received special attention over the last decades (Frank and Mestat [2000], Abchir [2016]), nevertheless, the design of piles still remains quite a complex task due to the nature of the problem (Terzaghi [1943], Fleming et al. [2008]). Soil mechanics theory is not always taken into consideration in the proposed formulas and even if it does, formulations are characterized from empirical relations and correlation with experimental data (Costa Aguiar [2008]). To all these approximations and uncertainties, one has to add the fact that the definition of soil characteristics remains a very complex task.

More importantly, theoretical formulations are mainly focused on the estimation of bearing capacity for the pile, while in most cases the critical "quantity of interest" of the problem is pile displacement. The increase of computational power came with the development of several numerical methods that try to properly model pile-soil interaction and estimate the global response of the system.

These numerical tools can be of great importance in an industrial environment where they can serve as a support for the design and analysis of geotechnical structures in earthquake engineering. Therefore, for applications considering nuclear installations, it is the role of EDF R&D to provide validated methodologies based on numerical simulations.

1.2 Objectives

The main objectives of this internship is the numerical evaluation of different modeling strategies of nonlinear pile-soil interaction. The analyses conducted focus on different types of loading, and take into account important aspects of pile-soil behavior, such as :

- non-linear behavior of unilateral friction in pile-soil interface ;
- non-linear behavior of soil at the base of the pile ;
- non-linear behavior of soil around the pile ;
- impact of installation procedure

1.3 Scope of the work

This work consists of six main chapters. In Chapter 2 the theoretical background for soil mechanics and foundation engineering is provided. The first part is dedicated to the existing constitutive models for soil mechanics. A general discussion is provided so as to better understand the difficulties of the analysis while at the end of this part two constitutive laws that were used in the framework of this internship are detailed. General definitions on foundation and a more specific discussion on bearing capacity as it was defined by Terzaghi [1943] are given. The last part of this chapter presents a literature review of the existing methods for single pile design under axial and lateral loading.

Chapter 3 introduces the numerical model used in the framework of finite elements analysis with code_aster. Important aspects of the model are explained with the focus on joint elements (R7.01.25 [2016]), that serve as the pile-soil interface and thus, have a primordial role in our analysis. Modelling procedure as well as important assumptions made for numerical applications are discussed in Chapter 4.

Chapters 5, 6, and 7 are dedicated to the presentation of numerical results. Three cases are examined separately where axial monotone, lateral monotone and lateral cyclic loading are applied respectively. The main goals of those chapters are to evaluate :

- capabilities and limitations of the proposed model ;
- the impact of theoretical assumptions (soil behavior, initial stresses) ;
- the importance of a correct estimation of mechanical properties for pile and soil ;
- the impact of numerical parameters of the model in global system response ;

Main conclusions derived from this work are presented in Chapter 8, where important aspects of numerical modeling as well as capabilities and limitations of the proposed numerical model are discussed. Proposals and potential modifications of the model are also given as perspectives of this work in the final chapter.

2 Theoretical Background

The first chapter of this work is divided in three main parts, and provides the necessary theoretical background for the understanding of foundation engineering. Starting from a general point of view, in the first part, a brief discussion of soil constitutive laws is provided so as to facilitate the lecture for the following parts. Some basic definitions for foundations as well as the presentation of critical aspects of the subject are introduced in the second part. At this level, we also provide a demonstration of the methodology proposed by Terzaghi [1943] which led to the formulation of today's Eurocode 7 expressions. Finally, in the last and final part we present a literature review of the existing methods for the design of single piles under axial and lateral loading.

2.1 Constitutive Laws in Soil Mechanics

The first constitutive laws that were developed for geotechnical applications were based in the hypothesis of an elastic-perfectly plastic behavior for the soil. An initial linear part, observed for small levels of stress/strain was described by the Hooke's relation, though the second, and non-linear part was expressed through the perfectly plastic relation based on Coulomb's friction theory. The combination of this two constitutive relations were formulated in a plasticity framework and is called Mohr-Coulomb model.

Even though, the Mohr-Coulomb criterion provides satisfactory results in some cases, it's capacity to properly predict soil behaviour for any loading conditions is quite limited. This is because of the complexity of soil media and the numerous factors that influence their behaviour. More precisely, as described in Huat [2009] these factors can be summarized as: 1) the existence of water (effective stress, pore pressure) ; 2) irreversible deformation ; 3) speed loading, strain level, soil density/permeability, and anisotropy that influence soil stiffness and strength, and ; 4) compaction, dilatancy, or consolidation state that can also have an important impact in soil behavior. To all these phenomena one has to add the impact of cyclic loading where a degradation of stress–strain and shear strength properties can be observed during loading cycles. Thus, it is quite evident, that soil behavior cannot be completely described using this constitutive law. For this reason, during these last decades and with the exponential growth of the computational power, several models have been developed for soil mechanics in the framework of the finite element analysis. Each of these models tries to properly describe some of the pre-mentioned aspects that influence soil behavior, however in some cases the proposed models are described through a great number of parameters that make their calibration quite a complicated task for the user.

Two different constitutive laws available on code_aster were used in this work : 1) Mohr-Coulomb and 2) Iwan's law. For a larger overview of other existing constitutive models the lecturer can refer to Huat [2009] and Lade [2005].

2.1.1 Mohr Coulomb

As already mentioned Mohr-Coulomb is one of the simplest elastic-perfectly plastic models that can describe soil behaviour. Elastic behavior is completely linear and the plastic part is described from a yield surface expressed in the principal stresses domain by equation 2.1:

$$F_{13}(\sigma_1, \sigma_3) = (\sigma_1 - \sigma_3) + (\sigma_1 + \sigma_3)\sin\phi - 2c\cos\phi = 0 \tag{2.1}$$

where, ϕ and c are the internal friction angle and the cohesion respectively. In the same way, the flow rule associated with the yield surface F_{13} is defined by equation 2.2:

$$G_{13}(\sigma_1, \sigma_3) = (\sigma_1 - \sigma_3) + (\sigma_1 + \sigma_3)\sin\psi - 2c\cos\psi \tag{2.2}$$

where ψ is the dilatancy angle. For the special case where $\phi = \psi$ the flow rule is associated and for any other case non-associated. A graphical representation of the yield surface of the model is given on Figure 1.

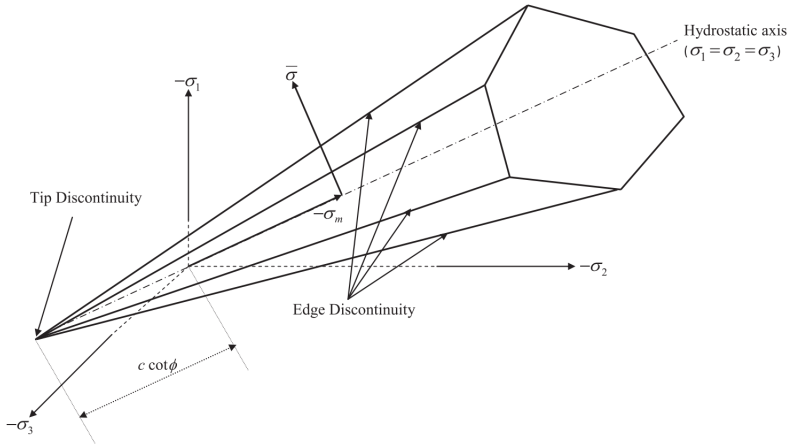

Figure 1: Mohr-Coulomb yield surface in the 3D principal stresses domain (2016).

It is important to state here that as seen from Figure 1 the yield surface of the model is discontinuous and thus numerical difficulties can appear during numerical integration of the constitutive law (non definition of the derivatives in the edges and tip discontinuity). More information on how to overcome this problem in code_aster can be found in R7.01.28 [2016].

2.1.2 Iwan's Law

Iwan's law is an elasto-plastic multimecanism constitutive model for the description of deviatoric cyclic behavior of geomaterials, based on linear kinematic hardening. The volumetric part is supposed completely elastic and thus the yield surface is expressed in deviatoric stresses as :

$$f_n = q_n - Y_n \tag{2.3}$$

where Y_n is a constant providing the yielding limit for the n mechanism and q_n is the deviatoric stress associated with the same mechanism.

Yielding limits Y_n and kinematic hardening parameters are computed through the degradation of the shear modulus G with the evolution of shear deformation γ. This progressive degradation is obtained through the hyperbolic equation 2.4, and is used in the definition of yielding limits Y_n :

$$G = \frac{G_{max}}{(1 - \frac{\gamma}{\gamma_{ref}})^n} \tag{2.4}$$

where G_{max} is the initial shear modulus, γ_{ref} is the shear deformation which generates $G = G_{max}/2$ and n is the exponential of the hyperbolic law. When in the calibration of the law, the relation between the evolution $G - \gamma$ can be obtained by calibrating the parameters of the model so as to reproduce the existing $G - \gamma$ curves that can be found in the literature for existing types of soil. A complete description of the model can be found in R7.01.38 [2017].

2.2 Deep Foundations

The main goal of this section is to introduce the principal aspects for the design of deep foundations. This section is divided in three main parts. In the first part some definitions and the mechanical functionality of this type of foundations are provided so as to facilitate the lecture of following sections. In the second part, the definition of bearing capacity as it was introduced by Terzaghi [1943] is provided so as to pinpoint the important aspects that have to be taken into consideration for the design of pile foundations. Finally, in the third and last part of this chapter we provide a description of important factors that influence the behavior of deep foundations as they were identified from several studies found in the literature.

2.2.1 Definitions on Deep Foundation

Deep foundations are footings that have a length greater than 10 times their width or diameter. Some classic examples of deep foundations are given in Figure 2.

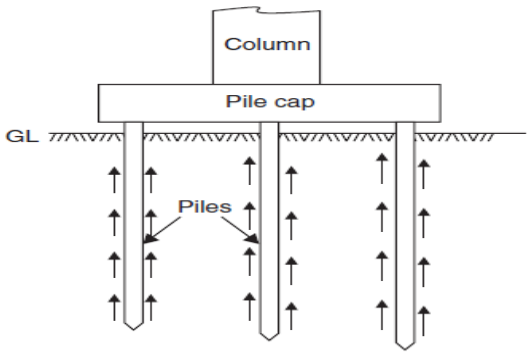

(a) Piles

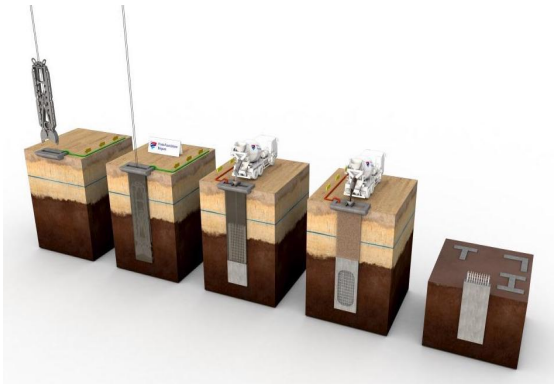

(b) Strip Piles

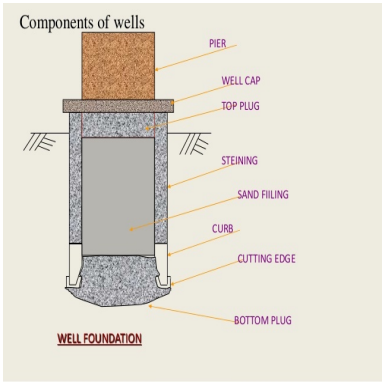

(c) Wells

Figure 2: Different types of deep foundations.

In the framework of this internship we are especially interested in pile foundation. Their use instead of shallow foundations is imposed either from the geotechnical constraints of a specific site, or from the "tolerated" level of displacement imposed for the superstructure. From a mechanical point of view, the main difference between shallow and deep foundations is the capacity of the latter to mobilize lateral friction so as to support the load of the superstructure. However, even for the specific case of piles we can distinguish two different types of mechanical functionality which are related to the specific geotechnical constraints of the site. More precisely, one can define :

- Friction or "Floating" piles : Piles that support the load of the superstructure through the mobilization of the lateral friction of the shaft.

- End-bearing piles : When a more rigid soil can be found in accessible depths a pile can search to transfer the load of the superstructure to the more resistant soil layer.

2.2.2 Bearing Capacity

The definition of bearing capacity for a footing was firstly introduced by Terzaghi [1943] in his pioneer work. His demonstration starts supposing a continuous shallow foundation ($D_f \leq B$) loaded with a vertical force Q (Figure 3a). The force exerted in the footing is transferred to the soil and one can define the critical load q_d, and thus the bearing capacity, as the maximum load per unit area, under which the supporting soil fails. Even though, this definition "seems" quite clear, special attention needs to be taken for different types of soil. More precisely, considering the settlement curve (settlement - load per unite area) in Figure 3b two different cases can be distinguished : 1) for a dense or stiff soil it exists a tangent line (C_1) which clearly defines the critical load q_{d1}; 2) for loose or fairly soft soils, there is no clear definition of a critical load. In the second case the critical load q_{d2} (C_2) is defined as the load value for which the load-settlement relation is approximately linear.

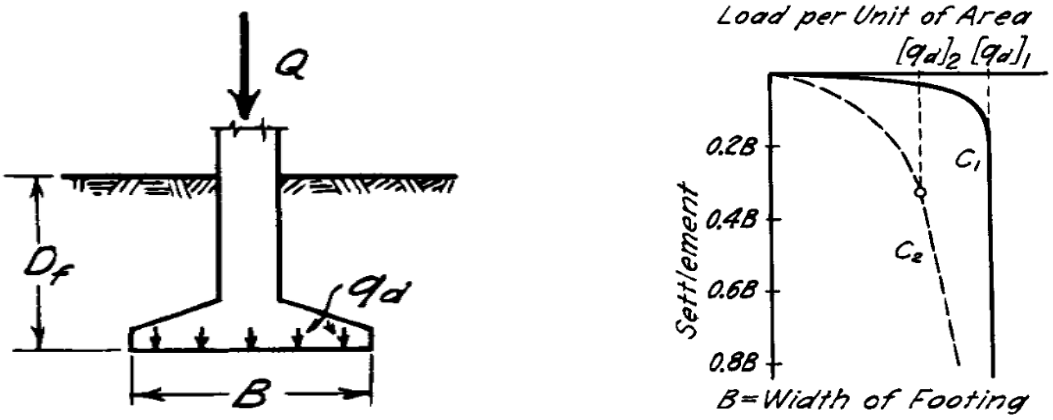

(a) Section of shallow footing. (b) Settlement curve.

Figure 3: Bearing capacity of shallow foundations (Terzaghi et al. [1996]).

The theoretical framework for the definition of bearing capacity of a shallow foundation is formulated through the theory of plastic equilibrium for the supporting soil. The method admits a rupture surface of an "ideal material" for the supporting soil. This surface has the form of the surface $fede_1f_1$ in Figure 4 and provides the necessary boundary conditions for the analysis of the problem. More precisely, the bearing capacity of a shallow foundation is given as the sum of three different terms : 1) adhesion and cohesion of a weightless material without external load; 2) friction of a weightless media in addition of a surcharge q on the ground surface, and; 3) friction of a material possessing weight and carrying no surcharge. Given these assumptions, theoretical studies admitting the theorems of limit analysis provide the solutions for each type of problem (presented in Figure 4).

1. Weightless soil with no surcharge :
   As seen from Figure 4a, one can define three main zones when in soil failure. In zone I, due to friction and adhesion between the soil and the base of the footing a triangular wedge appears, which behaves elastically. The boundaries of the zone form an angle of $45^o + \phi$ with the horizontal. Zone II is a zone of plastic flow, where radial shear is developed. The boundaries of the domain are on the form of a logarithmic spiral, the center of which is found in the outer edge of the base of the foundation. Finally, zone III is a zone of plastic flow where a plane shear pattern, identical to the

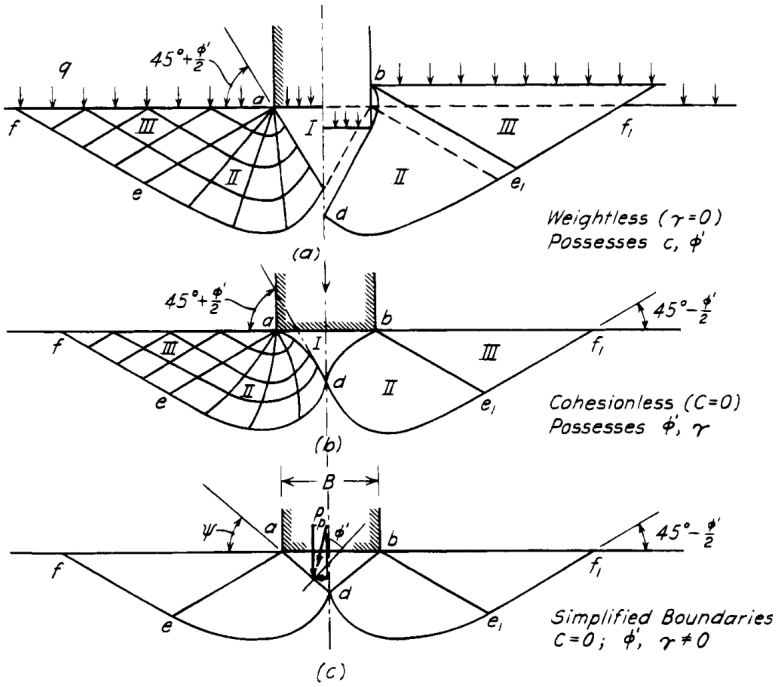

Figure 4: Plastic equilibrium zones in soil after failure (Terzaghi et al. [1996]).

one of the passive Rankine state, can be observed. In this zone, the boundaries of the domain consist of straight lines that form an angle of $45^o - \phi$ with the horizontal. The solution of this problem, according to Prandtl [1921], is given in the form of ;

$$q_c = cN_c \tag{2.5}$$

where c is the cohesion and N_c is the bearing capacity factor expressed as :

$$N_c = cot\phi \left[e^{\pi tan\phi} tan^2 \left(45^o + \frac{\phi}{2} \right) - 1 \right] \tag{2.6}$$

2. Weightless soil with surcharge :
For the case where a uniform surcharge q is supposed, Reissner (1924) has showed that bearing capacity increases by a factor qN_q and the expression for N_q is given from equation 2.7 :

$$N_q = e^{\pi tan\phi} tan^2 \left(45^o + \frac{\phi}{2} \right) \tag{2.7}$$

The combination of 2.7 and 2.6 postulates :

$$N_c = cot\phi(N_q - 1) \tag{2.8}$$

It is important to state here, that in general, shallow foundations are rarely in the surface of the soil. On the contrary they are normally found in a depth, D_f. Given this fact, we can admit that there always be a surcharge of the superficial soil that can be expressed as $q = \gamma D_f$ and thus the additional term in the bearing capacity for this problem takes the form of:

$$q_q = \gamma D_f N_q \tag{2.9}$$

3. Soil with weight and friction :
When in a cohesionless soil with no surcharge, no general solution exists for the

problem. The boundaries of the plastic equilibrium zones are shown in Figure 4b. The once straight lines of zone I as well as the once radial lines of zone II are now curved but the shear pattern of zone III is identical to the one described from the passive Rankine state.

So as to treat this problem and be able to provide a solution, an approximation is taken into consideration. More precisely, we now consider the case presented in Figure 4c, where the once curved lines are replaced by straight lines forming an angle ψ with the horizontal. The analysis now is focused on the research of a force P_p exerted in the edges ad, bd in the moment of failure. This force, which is equal to the passive earth pressure, is formed in an angle ϕ to the normal on the edge because of the slip occurring along these edges. The equilibrium of the wedge, without weight consideration, postulates that :

$$Q = 2P_p cos(\psi - \phi) \tag{2.10}$$

Supposing the average vertical pressure we define then :

$$q_\gamma = \frac{Q}{B} = \frac{2P_p}{B} cos(\psi - \phi) \tag{2.11}$$

Consequently, the problem postulates that we have to determine the value of P_p. If we define :

$$N_\gamma = \frac{4P_p}{\gamma B^2} cos(\psi - \phi) \tag{2.12}$$

The equation 2.11 takes now the form :

$$q_\gamma = \frac{1}{2}\gamma B N_\gamma \tag{2.13}$$

It is important to state here, that the unknown in equation 2.13 is the angle ψ. When in the calculation of the term q_γ then, for a given angle ϕ one must repeat the computation until the minimization of N_γ.

Given the aforementioned analysis, the expression of bearing capacity for a shallow foundation is obtained by the combination of equations 2.5, 2.9, and 2.13 :

$$\begin{aligned} q_d &= q_c + q_q + q_\gamma \Rightarrow \\ q_d &= cN_c + \gamma D_f N_q + \frac{1}{2}\gamma B N_\gamma \end{aligned} \tag{2.14}$$

In an equivalent way, Terzaghi (1943) introduces the bearing capacity for a pile foundation given as :

$$\begin{aligned} Q_d &= Q_p + Q_s \Rightarrow \\ Q_d &= q_p A_p + C f_s D_f \end{aligned} \tag{2.15}$$

Where, q_p is the bearing capacity of the point, A_p is the section of the pile, C is the circumference of the pile, D_f is the depth, and f_s is the average value of friction and adhesion per unit area of the pile-soil interface.

The major difference between equations 2.14 and 2.15 is the existence of the friction term in the definition of bearing capacity in piles. In addition, considering the estimation of end-bearing capacity in piles, several others exist in the literature proposed by other authors. Their main difference as can be seen in Figure 5 is the choice of the plastic zone that is considered for the failure of the soil (Meyerhof [1951], Cheng [2004], and Vesic

[1973]). According to the chosen plastic zone, a difference in the expression of N_q, N_c, and N_γ is obtained.

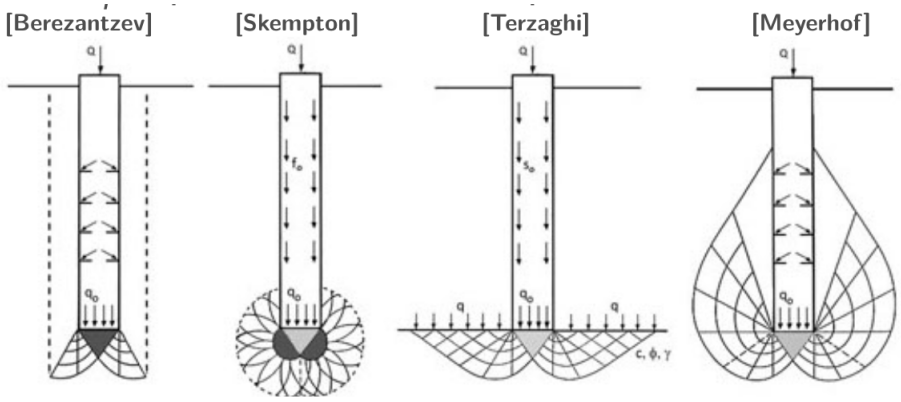

Figure 5: Boundary conditions for plastic zone soil's failure.

However, as explained by Terzaghi et al. [1996], the aforementioned theories are based in important assumptions such as : 1) the "ideal" rupture surface adopted in Figure 4 and 5; 2) no consideration of the depth of the foundation D_f, the soil weight γ, and the real distribution of vertical and horizontal forces in the expression of bearing capacity, and; 3) the hypothesis of a constant soil volume before failure. Nevertheless, given the uncertainties of the problem related to the difficulty in the definition of mechanical characteristics of soil, these approximations consist acceptable solutions for applied engineering.

2.2.3 Factors that influence pile behaviour

The main factors affecting the mechanical behavior of piles are the following :

2.2.3.1 Installation effects

Construction mode is of primordial importance in the design of pile foundations. Two different types of piles can be distinguished : 1) displacement (driven, bored) and ; 2) non-displacement (drilled) piles. The impact on each type of construction mode can be distinguished in two main categories :

1. Impact on Soil State :
   A change in the soil state can be observed according to the construction mode, related to displacement, deformation and compaction of the soil media.

   - Displacement Piles :
     For driven piles in sandy soil, Shakhirev et al. [1996] have observed the creation of two zones (Figure 6) in the soil media : 1) a zone of compaction and densification (Zone 1) and ; 2) a zone where the soil is "pushed up" (Zone 2). Shakirev relates the compaction zone to the combination of the compression of the pile head, as well as the lateral friction which generates a vertical down-going force in the sides. This compacted area, that grows bigger with the depth (in a radial sense), has as a result the "push up" of the superior soil layers of the same lateral distance. According to Shakhirev et al. [1996], the dimensions of zone 2 decrease in comparison to zone 1, with the evolution of the driving procedure of the pile.

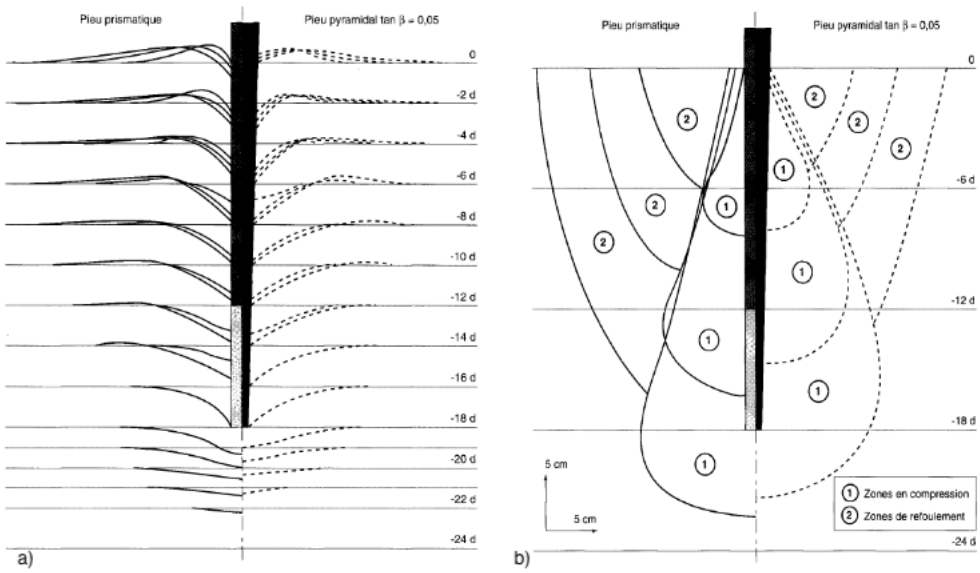

Figure 6: Driven pile in sandy soil, vertical : a) deformation, b) displacement.

For the case of clay media, Shakhirev et al. [1996] have observed a different behavior comparing to sand. More precisely, as can be observed in Figure 7, the compaction zone (Zone 1) has a more cylindrical shape and the influence depth at the head is more important than the radial dimension. This is related, according to Shakirev, to the incapacity of clays to redistribute the stresses in the media. This localization of stresses, can lead then to an earlier failure of the soil in the case of clay media and one can conclude that bearing capacity of displacement piles in sands is higher than the one in clays.

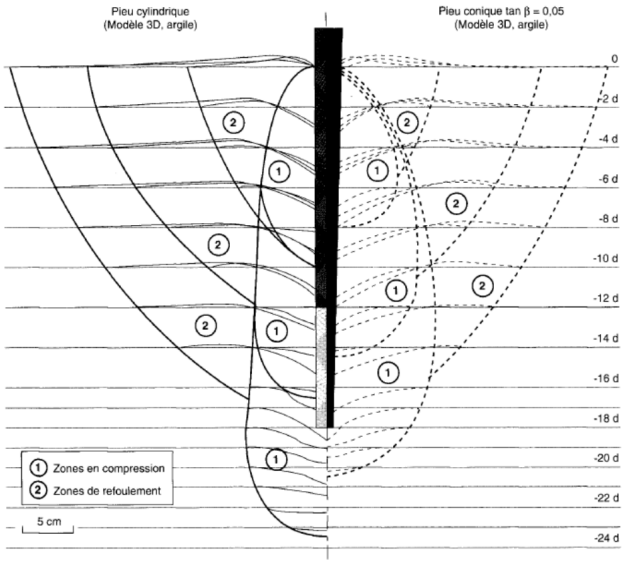

Figure 7: Deformation zones for the case of clay soil (Shakhirev et al. [1996]).

- Non-displacement piles :
  For the case of drilled piles, it is quite evident that the phenomenon of soil compaction is not present. On the contrary, Poulos and Davis [1980] have observed that when the drilling procedure is adopted for the construction of piles in sandy media, a relaxation of the soil in the head of the drill takes place. For this reason, Tomlinson and Boorman [2001] proposes the adoption

of the residual friction angle for the calculation of bearing capacity of piles. When in a clay media, Poulos and Davis [1980] have proposed the adoption of an adhesion coefficient between soil-pile which is lower than the undrained cohesion of soil before installation. This is due to the local increase of hydraulic pressure, yielded from the installation method, and which results on a local relaxation of soil. For a more detailed presentation concerning the installation effects of a pile one may refer to Abchir [2016].

2. Impact on Pile Capacity :
Pile capacity is influenced by soil state, as the lateral friction of the shaft (Q_s in equation 2.15) depends on the normal force exerted by the soil on the shaft.

For the case of a displacement pile, two different situation can be distinguished: 1) soil compaction causes an increase in the effective lateral stress exerted in the interface and thus an increase in lateral friction can be observed or; 2) the installation procedure causes a relaxation of lateral effective stress and thus a decrease in friction capacity. This second case is known in the literature as friction fatigue or "h/r" effect and was firstly observed by Vesic (1970) who showed that friction capacity at a specific horizon varies according to the driving procedure. The main causes of this effect can be summarized in Figure 8 and include : 1) free surface effect; 2) lateral pile movement; 3) history of soil stress, and; 4) history of cyclic load. For more information concerning friction fatigue one may refer to Costa Aguiar [2008].

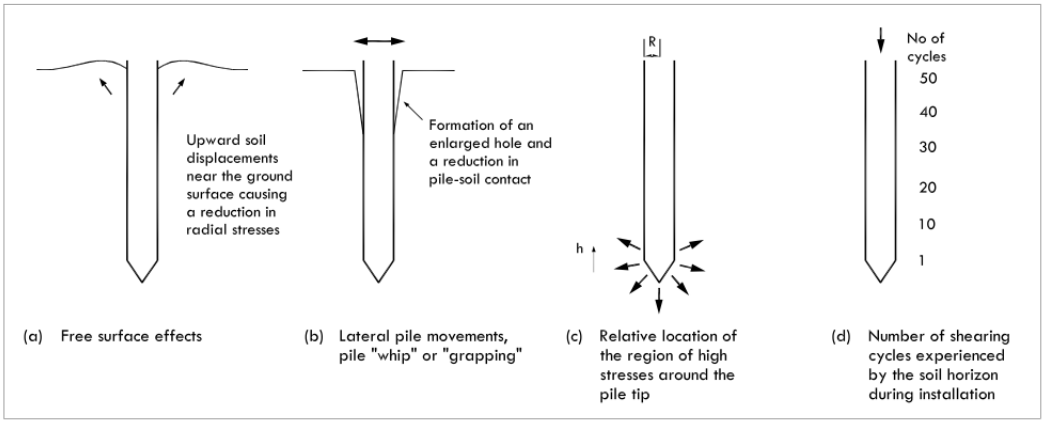

Figure 8: Friction fatigue causes after Chow [1997] (adapted from Costa Aguiar [2008]).

The numerical modelling of the installation procedure still remains limited due to the complexity of the phenomenon : 1) formulation in finite displacement, deformation and rotation; 2) dynamic nature of driven piles, or 3) water flow during the pile installation. Two different modelling methods that allow to take into consideration installation effects:

- Implicit modelling : Installations are taken into account through the consideration of friction fatigue during installation and thus a modification of the stress state around the pile (Said [2006]).
- Explicit modelling : Installation effects are taken into account explicitly through a full finite element model (Sheng et al. [2005], Todo-Bom [2014]).

2.2.3.2 Construction Material

Construction material is also a very important parameter that influences pile capacity. Piles can be constructed using wood, still, or concrete and considering the different types

of material a difference in behavior can be observed. More precisely, the type of material has an important impact in pile stiffness. For the case of a slender pile in a soil with a softening behavior, Randolph (1983) has showed that soil failure can be provoked in soil layers that are closer to the surface while the inferior soil layers are still intact (Figure 9).

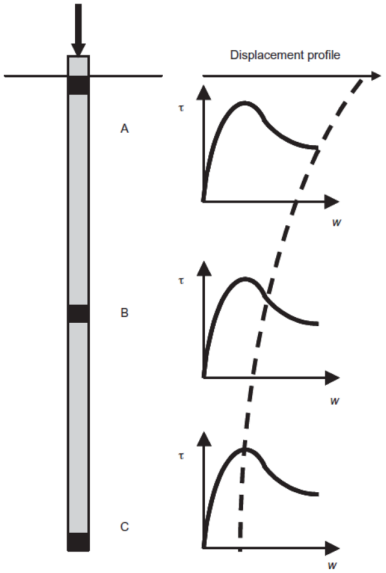

Figure 9: Progressive failure of soil along the pile profile (Randolph [1983]).

This phenomenon is due to pile deformation that leads to important relative displacement between pile and soil on the upper layers. On the contrary, for the case of a rigid pile the movement of pile is homogeneous and thus failure comes simultaneously for the total length of the pile.

Finally, construction material has an impact in the friction angle of the pile-soil interface. For example, in the case of steel piles corrosion takes place with time and thus a stronger bonding is created in the interface.

2.2.3.3 Time Effect

The last parameter that influences pile behavior is time after installation. Chow [1997] has observed the evolution of bearing capacity in total terms, as well as in traction, for driven piles in sand. The measured bearing capacity was compared to the one measured in the first day after installation and as presented in Figure 10 both the total as well as the capacity in traction seem to increase with time.

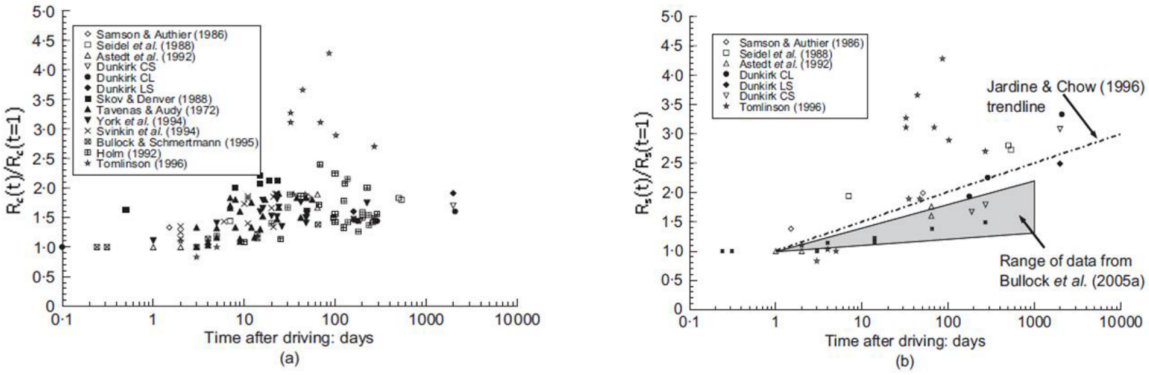

(a) Total bearing capacity R_c (b) Resistance in traction R_s

Figure 10: Evolution of bearing capacity of piles (Chow [1997]).

Three main causes have been identified and are responsible according to Chow [1997] for this increase :

- The corrosion of the interface that takes place during time increase the friction angle of the interface.
- Increase of effective stress around the pile related to the decrease of water pressure.
- Soil densification and thus increase of the shear strength of the sand.

2.3 Design Methods for Single Piles

In this final section a literature review is provided for the existing design methods of single piles. A distinction is made between axial and lateral capacity as well as between theoretical/empirical and numerical solutions proposed in the literature.

2.3.1 Empirical/Theoretical solutions - Axial capacity

As already seen in equation 2.15, axial capacity of piles is described from a friction term Q_s and a term related to end-bearing capacity Q_p. Several methods exist in the literature and allow to compute those two terms. A categorization of those methods, as it was proposed by Poulos [1989] can be found in Table 1. According to this table, three main categories can be defined. Category 1 and 2 consist of empirical solutions that do not take into consideration soil mechanics principles. The main idea behind these methods is the definition of problem's parameters through the correlation with existing data sets obtained *in-situ* or in laboratory (API [2011], AFNOR [2012], Abchir [2016]). Category 3 consists of more elaborated solutions that properly model soil behavior and that are developed in the framework of numerical analysis with the finite or boundary element methods (FEM, BEM).

Category	Axial Pile Capacity	Settlement
1	Correlations with CPT Correlations with SPT Total stress αmethod	Approximate correlations with pile diameter Column deflection multiplied by a factor
2A	Effective stress β method	Elastic solutions
2B	Effective stress method	Elastic solutions modified for slip
3A	Plasticity solutions for end-bearing capacity	Elastic finite element solution
3B	Non-linear load transfer analysis	
	Non-linear boundary element analysis Non-linear finite element analysis	
3C	Finite element analysis including simulations of pile installation	

Table 1: Categorization of existing methods for definition of axial capacity of piles (after Poulos [1989]).

As previously discussed (section 2.2.3.1), pile capacity is different according to the type of installation as well as the type of soil that is found in site. More precisely, Fleming et al. [2008] presented that bearing capacity for cohesive soils is principally described through the estimation of the capacity in friction, when for non cohesive soils, end-bearing capacity is a predominant percentage of total capacity.

2.3.2 Empirical/Theoretical solutions - Lateral capacity

When in the choice of a pile foundation for the support of a surcharge, the design of the foundation is mainly focused in the definition of vertical capacity. This is because the exerted vertical load is in general, more important than the horizontal one. Moreover, piles are usually constructed with an inclination to the horizontal, and thus we suppose that horizontal loads are taken by the horizontal component generated from the inclination of the pile. These two facts can make us believe that the estimation of lateral capacity of a pile is "unnecessary". However, the estimation of this lateral capacity can be of great interest in several cases : 1) when piles are forced in a vertical sense (pile walls), or; 2) when the construction of the more expensive "battered" piles can be avoided.

Pile design for lateral loading necessitates an *a priori* understanding of the failure mechanisms that can take place. More precisely, as we can see in Figure 11, two different mechanisms of failure can be observed. For short and rigid piles, a rotation of rigid body is observed. Passive earth pressure takes place in the right side of the soil above the rotation center as well as in the left side below the rotation center. For long piles, the mechanism of collapse supposes the formation of a plastic hinge in a certain pile section, and as a result, rotation takes place in the upper part of the pile according to the load. In this case the estimation of lateral capacity is only based to the limiting pressure of the upper part, because it is this part that controls pile failure.

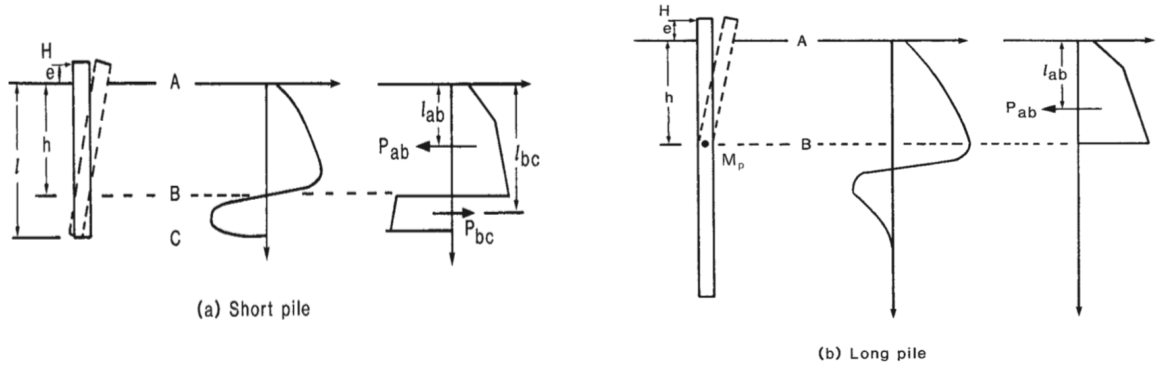

Figure 11: Failure mechanisms for lateral loading (Fleming et al. [2008]).

Broms [1964a,b], studied the response of piles in lateral loading for the case of cohesive and cohesionless soils, by distinguishing different case studies (short/long piles, free/fixed head piles, and their combinations). Other approaches can be found in Reese et al. [2002], and Fleming et al. [2008].

2.3.3 Numerical Solutions

The theoretical and empirical solutions mentioned in the previous section, provide an estimation of the axial or lateral capacity of piles but in terms of bearing capacity. These methods that are largely used in construction engineering, do not provide any information on settlement of pile or deformation of the surrounding soil. This aspect is a considerable drawback of these methods, as in some cases important displacements can be observed for a pile foundation. For this reason more rigorous methods that properly estimate the settlement for a given load (*settlement curves*) were developed.

2.3.3.1 Load transfer method

The principle idea behind the load transfer method is to represent the soil surrounding the pile as a series of identical but mutually independent springs (Winkler model) (Figure 13a).

Each spring has it's own stiffness, k, that relates displacement with load per unit length, and that is usually referred in the literature as the coefficient of subgrade reaction (Terzaghi [1955]). Given the value of this coefficient (constant or linear evolution with depth) the method allows the evaluation of internal forces and displacements for the pile.

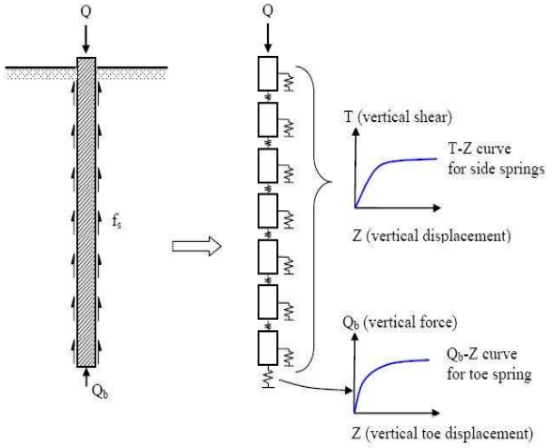

(a) Problem Discretization (Costa Aguiar [2008]).

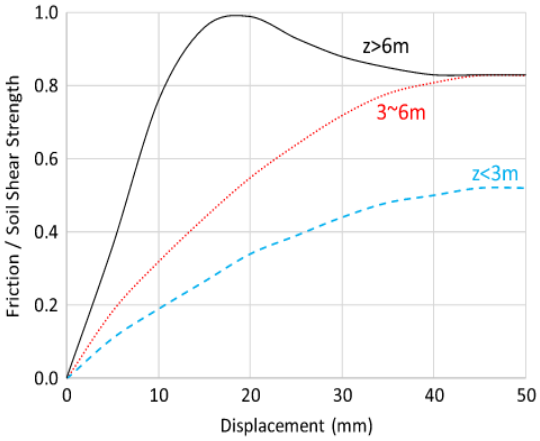

(b) Pile friction/shear strength for steel piles in clay (adapted from Dias and Bezuijen [2017]).

Figure 12: Load transfer method.

An amelioration of the Winkler method was adopted by Coyle and Reese [1966], which leads in the so called load transfer method. The subgrade coefficients for the stiffness definition were completely replaced by complete expressions of load transfer ($t - z$ or $p - y$) curves for each spring. According to the type of loading, lateral spring behavior is expressed from : 1) a shear t, versus vertical head displacement z curve, for an axial load, or; 2) normal force p, versus deflection y for a lateral load.

When in the application of the method, the load transfer curves can be obtained from empirical relations or from full-scale load tests in piles. Different constitutive behavior and non-linear models can be applied to express soil behavior in each level. A proposed example (after Coyle and Reese [1966]), for piles in clays can be seen in Figure 13b and for more examples one may refer to Abchir [2016].

2.3.3.2 Elastic continuum methods

The modelling procedure with the elastic continuum method admits a continuous media for the soil domain. The method focuses in a small element of pile which is supposed to be uniformly loaded. The solution of the problem is obtained after a compatibility condition is imposed in the neighborhood of pile and soil. More precisely, supposing a given axial load acting in a compressible pile, one can define pile displacement. Soil displacement can be obtained through the Mindlin equations and a compatibility condition reads that, when the pile soil behavior stays elastic, the two calculated displacements have to be equal. Poulos and Davis [1980] have modified the initial method so as to take into account pile in homogeneity and slippage of the interface.

2.3.3.3 Boundary element method

Boundary element method supposes a complete separation of the pile-soil media. Soil's behavior and characteristics are expressed in the model through the pile soil interface. The solution of the problem is usually obtained supposing a substructure technique that allows to separate the problem. More precisely, the initial structure is divided in small substructures and each one of them is solved independently. Final solution is obtained

through linear superposition of all solutions. Just like the elastic continuum method a compatibility condition is necessary so as to determine the contact of the two "bodies" (Poulos and Davis [1968]).

2.3.3.4 Finite element method

Finite element method is one of the most commonly used methods for the modelling of pile-soil response. It's popularity, with the scientific and construction community, lies with the possibilities that offers to the user, to properly model the non linear behavior of all the components of the problem, as well as the ability to model complex geometries. Two main sources of non linearities can been distinguished for pile soil interaction : 1) non-linear behavior of soil, and ; 2) non linear behavior of pile-soil interface. For the case of soil behavior section 2.1 presented several elasto-plastic laws to model the non linear phenomena in soil. When in the modelling of pile-soil interface, with FEM, the most common strategies proposed in the literature are based on the use of specific types of elements known as "joint elements". Several versions of these elements have been proposed in the literature. For reasons of completeness we simply cite here the existence of : 1) "zero-thickness" elements (Cerfontaine et al. [2015]); 2) "thin-layer" elements (Sharma and Desai [1992]), and; 3) "hybrid" elements (Villard [1996]).

Other types of modelling with FEM found in the literature propose a "simplified" version of the pile represented with a macro-element (Grange et al. [2009], Lysmer et al. [1981]).

2.4 Concluding remarks

The present chapter provides an overview of important aspects regarding pile foundations and mechanical behavior of soils.

Constitutive laws are not capable to properly model all physical phenomena but approximations are proposed according to the case study. In this work, Mohr-Coulomb model and Iwan's law were chosen to model soil's non-linear behavior.

The estimation of bearing capacity of footings is formulated in the framework of plastic equilibrium for the soil, and is based on several hypothesis of simplification of the problem. According to Terzaghi [1943], these are acceptable in regard to the great marge of error in estimation of soil's mechanical characteristics. Bearing capacity of pile is defined as the sum of lateral friction of the shaft and end-bearing capacity at the base of the pile. It arises from different literature studies that important factors influencing pile capacity are the installation mode, construction material as well as the time after construction.

Single pile design methods can be distinguished in empirical/theoretical and numerical ones. Empirical solutions consist of approximations of bearing capacity, based on correlations with existing *in-situ*, or laboratory test results. Soil's mechanical properties are not taken into consideration in formulas and important aspects such as installation method are implicitly taken into account with the use of corrective coefficients. Numerical solutions focus on the estimation of load-settlement curves for the pile. Different methods are proposed in the literature, while the most common remain load transfer method. The introduction of the proposed numerical model, in the framework of finite elements analysis is the subject of the following chapter.

3 Numerical model for pile-soil interaction

The numerical method adopted in the framework of this internship is the finite element method (FEM) with code_aster. A full-FEM 3D model for a cylindrical pile is proposed, where soil and pile are explicitly modelled. The geometry of the domain is provided via the Salome-Meca software, where we can define the external boundaries of the semi-finite domain, soil stratification, pile diameter and length, as well as the elements that are going to serve as the interface between pile and soil.

In terms of finite elements the model consists of : 1) 3D 8-node hexahedric elements representing the soil; 2) Euler-Bernouli beam elements representing the pile, and; 3) joint elements for the modelling of the interface (Figure 13a). The particular choice of beam elements for the representation of pile behavior is based on previous analysis realized at EDF R&D, which showed that beam elements facilitate the calculation of internal forces in the pile, comparing to 3D volumetric elements.

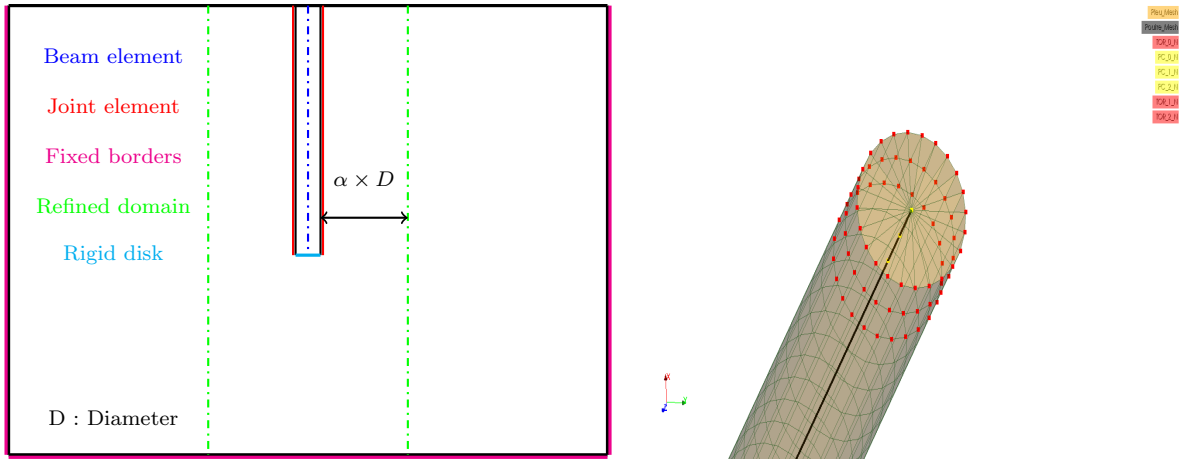

(a) Schematic view of the numerical model. (b) Detail on kinematic relations.

Figure 13: Numerical model.

Continuity of the model is obtained by imposing equal displacement relations between the nodes of the beam (yellow nodes PC_i_N in Figure 13b) and the external nodes at the circumference of the pile situated in the same vertical z coordinate (red nodes TOR_i_N in Figure 13b). At pile head beam elements arrive at a rigid disk allowing to better distribute stresses at the head and thus better approximate the physical behavior. Green domain defined in Figure 13a is a refined domain of dimension $\alpha \times D$, where D pile diameter. This domain is used so as to refine the discretization of the medium only in a specific region where it actually has an impact in results. An example of the obtained mesh for $\alpha = 2D$ is given in Figure 14.

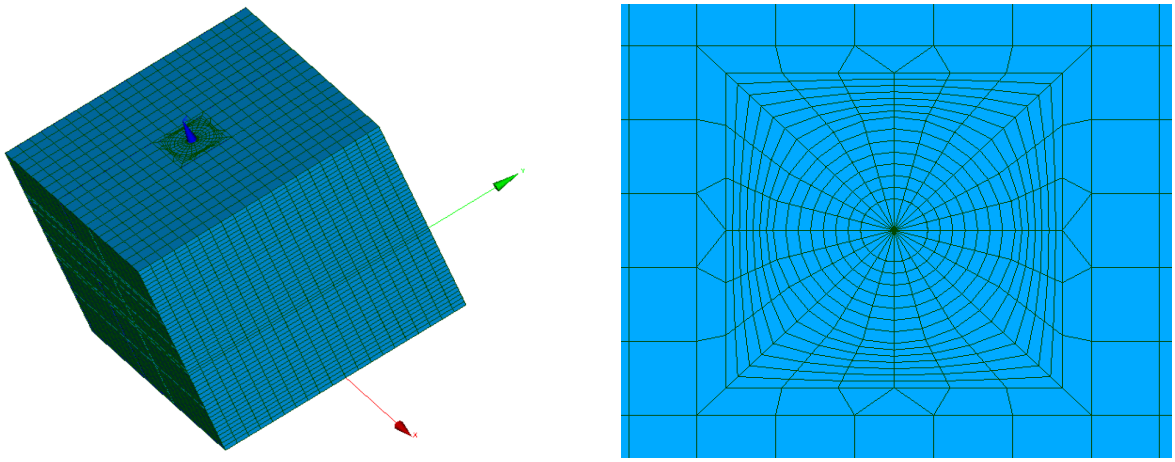

(a) 3D view. (b) Detail on the refined area.

Figure 14: Discretization of the domain.

3.1 Joint elements

Joint elements are used in the model so as to represent the non-linearity of the lateral friction on the pile-soil interface. Joint elements implemented in code_aster (`JOINT_MECA_FROT`) are "thin-layer" elements where a small thickness can be defined (R7.01.25 [2016]).

3.1.1 Signorini conditions for unilateral contact

The contact conditions adopted for joint elements are defined from the Signorini conditions of unilateral contact.

- $\sigma_N \leq R_t$ (Normal reaction on the interface)
  The normal reaction σ_N to the interface can take values that are smaller than resistance in traction R_t. If in contact $\sigma_N < R_t$. If not $\sigma_N = 0$.
- $\delta_N \geq 0$ (Impenetrability condition)
  If the two bodies are in contact normal displacement $\delta_N < 0$. If not $\delta_N = 0$.
- $\sigma_N \times \delta_N = 0$ (Equivalent of the consistency condition in plasticity)
  This expressions takes the place of the Kuhn-Tucker conditions.

A graphical representation of the condition applied to the reactions is given with Figure 15, where f_T is the shear resistance.

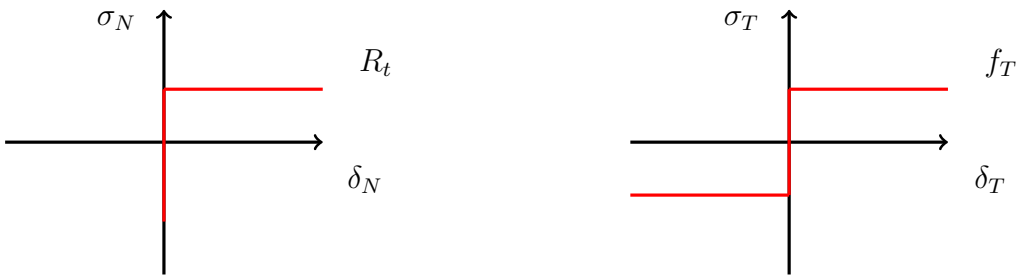

(a) Normal component. (b) Tangential component.

Figure 15: Graphical representation of the *Signorini* conditions.

Numerical problems may occur when directly applying the Signorini conditions, due to the non existence of the derivatives of the normal as well as the tangential component. Therefore, special numerical procedure has to be applied so as to overcome this problem.

3.1.1.1 Lagrange multipliers method

Lagrange multipliers methods, is based in the definition of certain multipliers λ, that admit duality condition with the displacement (or reactions) of the problem. A reformulation of the Signorini conditions in this framework, reads :

$$\delta_N \geq 0, \quad \lambda \leq R_t, \quad \delta_N \times \lambda = 0 \tag{3.1}$$

The resolution of the problem for each calculation instant is given by imposing the condition of relative displacement equal to zero ($\delta_N = 0, \lambda \neq 0$).

For the case of static loading, the method is quite efficient. However, for the dynamic case possible problems may occur due to the non well definition of velocity $\dot{\delta}$. For example, we considere the Newmark integration scheme described as :

$$\begin{aligned} \delta_{n+1} &= \delta_n + \dot{\delta}_n \Delta t + \left[\left(\frac{1}{2} - \beta \right) \ddot{\delta}_n + \beta \ddot{\delta}_{n+1} \right] \Delta t^2 \\ \dot{\delta}_{n+1} &= \dot{\delta}_n + [(1-\gamma)\ddot{\delta}_n + \gamma \ddot{\delta}_{n+1}] \Delta t \end{aligned} \tag{3.2}$$

Or equivalently, one can wright :

$$\begin{aligned} \ddot{\delta}_{n+1} &= \frac{1}{\beta \Delta t^2}(\delta_{n+1} - \delta_n) - \frac{1}{\beta \Delta t}\dot{\delta}_n - \left(\frac{1-2\beta}{2\beta} \right) \ddot{\delta}_n \\ \dot{\delta}_{n+1} &= \frac{\gamma}{\beta \Delta t}(\delta_{n+1} - \delta_n) + \left(1 - \frac{\gamma}{\beta} \right) \dot{\delta}_n - \Delta t \left(1 - \frac{\gamma}{2\beta} \right) \ddot{\delta}_{n+1} \end{aligned} \tag{3.3}$$

Supposing the specific parameters $\beta = \frac{1}{4}$, and $\gamma = \frac{1}{2}$, as well as $\delta_{n+1} = \delta_n$ (imposed displacements), the second equation of the system 3.3 reads $\dot{\delta}_{n+1} = -\dot{\delta}_n$. This means that oscillations can be observed in the definition of velocity. A remedy for this problem can be obtained with the correction of the velocity filed after convergence.

3.1.1.2 Penalty method

The penalty method is the one that is used in code_aster and consists of an approximation of the Signorini conditions (Figure 16). More precisely, an imposed stiffness allows us to express stresses as :

$$\begin{aligned} \sigma_N &= K_N^{imp} \delta_N \\ \sigma_T &= K_T^{imp} \delta_T \end{aligned} \tag{3.4}$$

This way, the derivatives can be normally computed and thus the implementation of the model becomes easier.

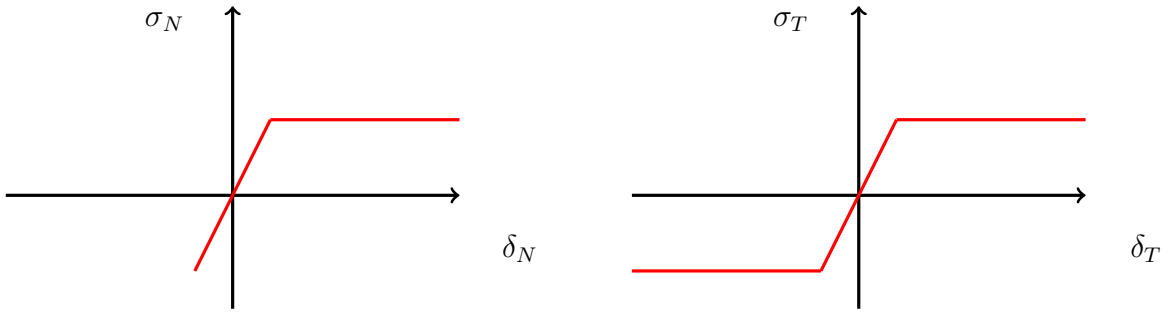

(a) Normal component. (b) Tangential component.

Figure 16: Graphical representation of the penalty method for the approximation of Signorini conditions.

3.1.2 Constitutive behavior of joint elements

The constitutive law, supposed for the joints is the Mohr-Coulomb criterion described in chapter 2.1.1. According to this criterion, tangential and normal components of stress, are related through the tangent of the friction angle (ϕ') of the interface $\mu = \tan\phi'$:

$$\|\tau\| = \mu \times \sigma_N \tag{3.5}$$

When in model calibration with joint elements, five parameters have to be defined : 1) K_N, and K_T the normal and tangential stiffness of the joints; 2) c, the adhesion of the joint; 3) μ the friction coefficient of the joint, and; 4) K a hardening parameter. It is important to state that traction resistance is given as $R_t = c/\mu$.

Concerning the plasticity theory for the joints, only the tangential part admits plastic deformations. Normal component is computed through elastic relations and thus we can define for the tangential part :

$$\begin{aligned} \delta_T &= \delta_T^{el} + \delta_T^{pl} \\ \sigma_T &= K_T \delta_T^{el} = K_T(\delta_T - \delta_T^{pl}) \\ \sigma_N &= min(K_N \delta_N, R_t) \end{aligned} \tag{3.6}$$

Given those parameters, the flow rule of the model is defined as :

$$\begin{aligned} f(\sigma,\lambda) &= \|\sigma_T\| + \mu\sigma_N - c - K\lambda \leq 0 \\ \dot{f} \times \dot{\lambda} &= 0; \dot{\lambda} \geq 0 \\ \dot{\delta_T^{pl}} &= \dot{\lambda}\frac{\sigma_T}{\|\sigma_T\|} \end{aligned} \tag{3.7}$$

While $f(\sigma,\lambda) < 0$ elastic behavior is supposed for the problem and thus $\delta_T^{pl} = 0$. When $f(\sigma,\lambda) = 0$ the plastic flow is activated and thus model behavior is computed through equations 3.7.

3.2 Concluding remarks

The present chapter introduces the numerical model used in the framework of this work. A full-FEM 3D model is proposed for the modelling of pile soil interaction. Pile is represented with beam elements that facilitate the computation of internal forces in the pile, while soil is represented with volumetric elements. Modelling of friction in the pile-soil interface is considered with the use of joint elements where the Mohr-Coulomb criterion of friction is implemented. Particular aspects of the proposed model as well as the modelling strategy and basic assumptions adopted in this work are the subject of the next chapter.

4 Modelling strategy for pile-soil interaction

The main goal of this chapter is to sum up the principal ideas followed during the numerical analysis. Different steps of numerical procedure are explained and main hypothesis are justified here so as to provide a global idea on the procedure before continuing with numerical results. We simply cite here that those numerical results consist of *in-situ* experimental campaigns where an axial, or lateral cyclic loading is applied.

4.1 Basic soil modeling assumptions

Different mechanisms of failure are due to different types of load applied in the structure, and thus, constitutive behavior of the model is considered according to the type of the applied load.

For axially loaded piles, the impact of non-linearities related to lateral friction, end-bearing capacity as well as their combination has to be examined. Soil media above pile base is supposed to be elastic and friction is modelled with joint elements, while soil below pile base is either elastic or non-linear for the case where end-bearing capacity is examined (Figure 17a).

For laterally loaded piles, non-linearities of lateral soil have to be examined. Soil below pile base is supposed to be elastic or non-linear (either way no impact is observed between these models) and soil above pile base is supposed non-linear (Figure 17b). Mohr-Coulomb and Iwan's law are tested so as to compare the results. Joint elements are used in this case so as to allow the opening of soil-pile interface. Especially for the case of Iwan's law, where traction and compression resistance are equal, the use of joints elements is necessary so as to allow pile-soil detachment and avoid non physical phenomena.

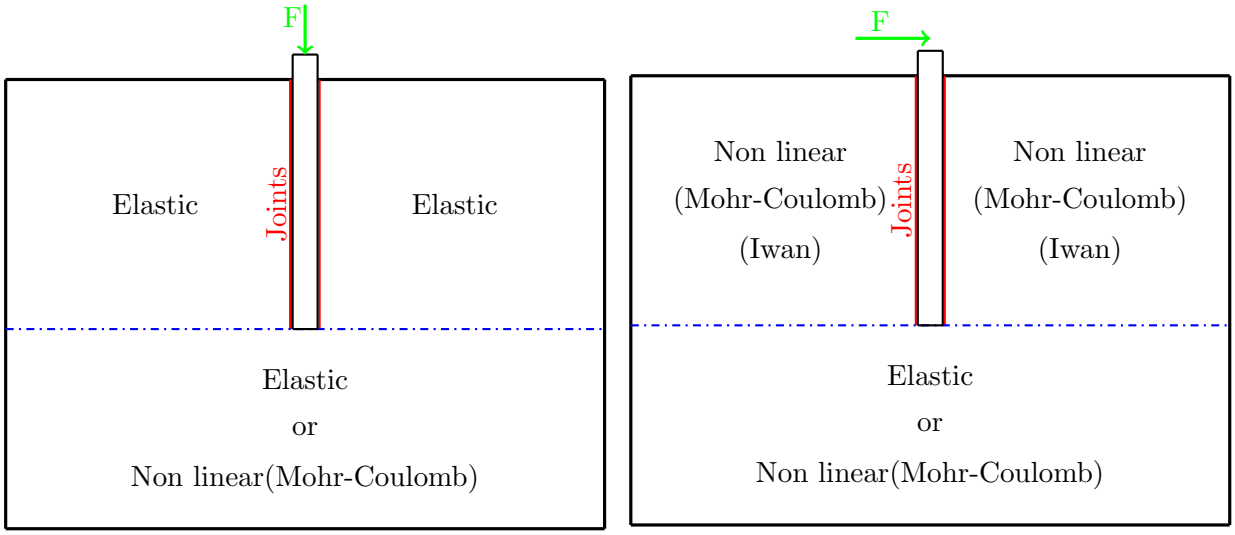

(a) Axial load. (b) Lateral load.

Figure 17: Constitutive behavior of soil according to load.

4.2 Definition of mechanical parameters

For all types of constitutive behavior that we use in code_aster, the minimum parameters necessary to define the elastic behavior are listed bellow :

- Young's modulus (E):
  A first estimation of Young modulus is taken from correlations available on the literature. When SPT results are provided, we can use the static cone resistance q_c

along with direct expressions for the estimation. Static cone resistance is related to dynamic cone resistance through equation 4.1 :

$$q_c = C \times q_d \tag{4.1}$$

where the values of C are obtained from Table 2.

Material	Above water table	Below water table
Silt	1	1.2 to 3
Sandy clay	0.5 to 0.9	0.1 to 0.4
Sand	1	-
Sand and gravels	1	1 to 2.6

Table 2: Values of C proposed by Cassan [1988] (adapted from Alves Fernandes [2014])

Given equation 4.1, C values and q_c we compute q_d and we use the direct expressions of Table 3 so as to estimate the elastic Young's Modulus.

Material	Analytic relation
Crushed graves	$E = 67.8 \times q_d^{0.55}$
Salty soils	$E = 53.7 \times \ln q_d + 9.1$
Clayed soils	$E = 35.9 \times \ln q_d + 21.2$
Plastic clayed soils	$E = 23.2 \times \ln q_d + 12.5$

Table 3: Direct relations between the dynamic cone resistance and the Young's Modulus proposed by Chua [1988] (adapted from Alves Fernandes [2014])

When no SPT data are available literature references with indicative values, are taken into consideration (Hunt [2005]).

- Poisson's ration (`NU`) :
  Fixed values of $\nu = 0.3$ and $\nu = 0.2$ are chosen for the soil, and pile respectively.
- Volumetric mass density (`RHO`):
  Values are fixed according to the specific unit weight of soil (γ) and equation 4.2.

$$\rho = \frac{\gamma}{g} \tag{4.2}$$

  Unit weight values are given in the case studies.

For non-linear constitutive laws, other parameters that need to be defined.

4.2.1 Mohr - Coulomb

Three parameters of the model have to be defined : 1) friction angle ϕ; 2) dilatancy angle ψ, and; 3) cohesion c_{mc}. Friction angle and cohesion for the soil are directly defined from soil characteristics provided in each case study. Dilatancy angle is taken equal to friction angle so as to decrease the number of unknowns.

4.2.2 Iwan's law

Two parameters have to be defined : 1) shear deformation γ_{ref}, and; 2) the exponential for the hyperbolic law, n (see also equation 2.4). Given the Young Modulus, Poisson's ratio and the level of deformation to be examined, a shear test is reproduced in code_aster (with the command `CALC_ESSAI_GEOMECA`), so as to calibrate the aforementioned parameters (γ_{ref}, and n) and generate the $G - \gamma$ curves proposed in the literature.

4.2.3 Joint elements

Joint elements constitutive behavior is described through five parameters. Three of them are completely related to the numerical treatment of the Signorini conditions without any physical meaning (K_N, K_T, K), while the rest of them (c, and μ) describe the physical side of the model. An "ideal situation" would be to somehow fix the values of non physical parameters in a way that joint behavior would be completely depended to physical ones. This is to be examined in the sensitivity study and according to loading conditions.

Physical values of the model are calibrated through soil parameters. Concerning the interface friction coefficient μ, it is standard practice to consider a percentage between 50% and 70% of the soil's internal friction angle. Adhesion supposed equal to soil cohesion.

4.3 Definition of initial stress field

The first step of modelling procedure is used to initialize the stress field at soil. For this reason vertical stresses are calculated through the classic expression :

$$\sigma_z(z) = \sigma_v(z) = \rho \times g \times z \tag{4.3}$$

where ρ, is the volumetric mass density of soil, g is gravity acceleration, and z is the depth from the surface. In the same way, we can define the horizontal initial stresses as :

$$\sigma'_h = K_0 \times \sigma'_v \tag{4.4}$$

where K_0 is the earth pressure at rest. An important remark is that the definition of K_0 is given in terms of effective stresses (σ'_v, and σ'_h) and thus the impact of water has to be taken into account :

$$\begin{aligned} \sigma'_v &= \sigma_v - \rho_w \times g \times z \Rightarrow \\ \sigma'_v &= \sigma_v - u \end{aligned} \tag{4.5}$$

where ρ_w is the volumetric mass density of water. For all numerical studies conducted during this internship, water pressure is only taken into account through equation 4.5 and no increase in pore pressure or water flow are supposed.

Equation 4.4 implies that the used earth pressure is equal to the one at rest for the soil. Despite the fact that this hypothesis do not consider the impact of pile installation (see also chapter 2.2.3), this modelling strategy is adopted in this work. For the case of sands, this earth pressure at rest can be expressed according to Jacky's rule as :

$$K_0 = 1 - \sin\phi \tag{4.6}$$

where ϕ is the internal friction angle for the soil. The impact of this choice is going to be examined thereafter, so as to pinpoint the importance of a correct estimation for the earth pressure.

After the initialization of initial stresses for the soil, a second computation takes place so as reinitialize displacements to zero and verify the stress field. Finally, the external load is applied.

4.4 Sensitivity study

A mesh dependency analysis takes place before every computation so as to define the size of discretization. When mesh dependency is studied the dimensions of the refined domain (value of α in Figure 13a) is supposed sufficiently large so as not to influence results. For a fixed mesh size, a sensitivity study concerning the size of the refined domain takes place. In both cases the global response of the system is examined so as to conclude with the choice of the size of refined domain and mesh.

In a next step, a parametric study concerning parameters of the joint elements (see also chapter 4.2) is conducted so as to evaluate the impact of each parameter in global response. Special attention is given in the influence of non physical parameters, whose calibration consists a complex task.

4.5 Model calibration

At first, a re-calibration of Young Modulus of soil takes place, so as to reproduce the elastic behavior of the experiment, and if this is deemed necessary. Unit weight γ, initial earth pressure K_0, and Poisson's ratio ν are taken intact as they were previously defined (sections 4.2, and 4.3). Two approaches are followed for the rest of the values.

- Numerical parameters of joint elements :
  A first numerical study adopts mechanical properties of soil as they were estimated from experimental procedures (section 4.2). Physical parameters of joints are taken as $\mu = 0.5$, to $0.7 \tan\phi$, and $c = c_{soil}$. A calibration of numerical parameters completes the study.

- Parameters of joints and soil (cohesion, friction angle) :
  Along with joint parameters, soil cohesion and friction angle are also changed so as to obtain the approximation of experimental data.

When axial load is applied three cases are examined : 1) elastic behavior; 2) lateral friction and elastic behavior for soil at base ; 3) perfect contact (no joints) and non-linear soil behavior at the base.

4.6 Concluding remarks

The present chapter provides an overview of important aspects regarding modeling strategy for pile-soil interaction.

It arises from the presented analysis that soil constitutive behavior is to be defined according to the type of the applied load. Two main cases for an axial and lateral load where distinguished and will be examined in the following.

When specific nonlinear material behavior is of interest, model parameters are the first to define before numerical computations. When no information are provided, standardized tests or literature references are used so as to estimate the necessary parameters. It is at this point where the need of quantification methods finds it's importance in the study. In this work literature references as well as correlation with SPT results will be used.

For a specific set of parameters, a sensitivity study allows the definition of mesh size and the borders of the refined domain. A parametric study follows so as to better understand the impact of each parameter of joint elements. This step is necessary for the final calibration of interface and soil parameters. In the following chapters different case studies are examined so as to evaluate the proposed numerical model.

5 Pile response to axial monotone loading

The reference case consists of an experimental campaign conducted by Briaud et al. [2000] in piles undergoing axial static loading.

5.1 Case study description

The pile tested by Briaud et al. [2000] was a cylindrical concrete bored pile with a length $L = 11.7$m and a diameter $D = 0.915$m. Young's Modulus and Poisson ratio are supposed to be $E_p = 26$GPa and $\nu_p = 0.2$ respectively. Soil media consists of several deposits whose geometry is presented in Figure 18. Water level is at a depth of 6.0m. The experimental campaign was conducted by imposing an increasing load at the head of the pile. However, in numerical study imposed displacements ($\delta = 15$mm) were chosen so as to facilitate convergence with the Mohr-Coulomb model (see section 6.1).

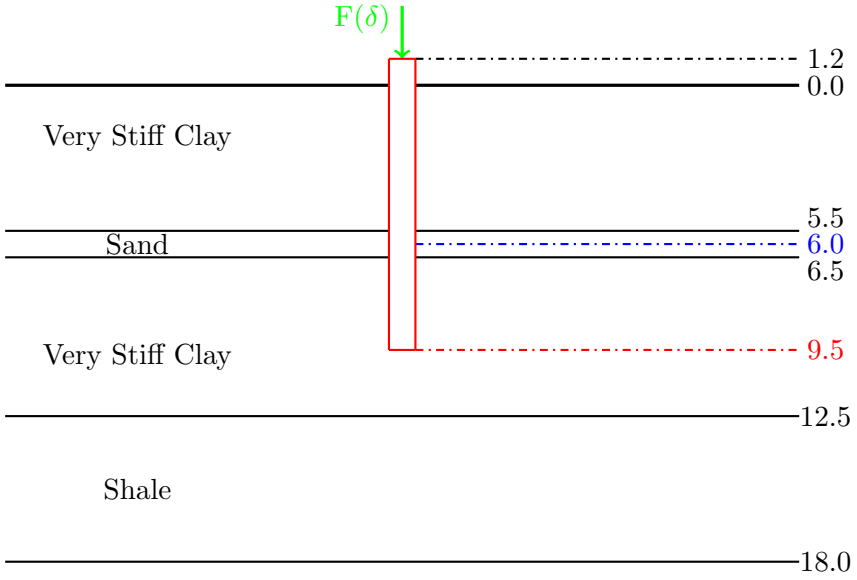

Figure 18: Geometry and mechanical characteristics of site (Briaud et al. [2000]).

For the axial case, soil behavior is adopted from Figure 17a where soil below pile head is modeled with the Mohr-Coulomb criterion.

5.2 Mechanical characteristics of soil

Not all the necessary mechanical characteristics of soil were provided in the experimental study and thus assumptions have to be made with respect to chapter 4.2. Given the values of shear strength S_u measured in the site (Table 4), an estimation of the Young's Modulus for layers of very stiff clay can be obtained from equation 5.1 according to Hunt [2005].

$$E_s = 1500 \times S_u \tag{5.1}$$

For the case of sand and shale, limit values for E_s were obtained from the same source (Hunt [2005]). Those values along with the given values of friction angle, unit weight, earth pressure (adapted from equation 4.6) and cohesion are presented in Table 4. Values with bold font were not provided and thus they were chosen from the literature.

	S_u [kPa]	E_s [MPa]	ϕ [^{o}]	γ [kN/m^3]	c [Pa]	K_0
Very Stiff Clay	110	**165**	20	19.6	13 $\times 10^3$	**0.65**
Sand	-	**50**	**34**	**20**	**100**	**0.44**
Very Stiff Clay	160	**210**	26.5	19.5	57 $\times 10^3$	**0.55**
Shale	-	**4000**	**26**	18.9	**70** $\times$ **10^3**	**0.53**

Table 4: Initial parameters of the numerical model.

5.3 Mesh dependency

The results of the mesh dependency analysis, are given in Figure 19. For those first studies mechanical characteristics of soil are adopted from Table 4. Parameters of joint elements are fixed as followed : $K_N = K_T = 10^9$Pa, $K = 10^6$Pa, $\mu = 0.6 \times \tan\phi$, and $c = c_{soil}$. Dilatancy angle for Mohr-Coulomb criterion is equal to friction angle.

According to Figure 19, a stabilization of the results is obtained for 41760 number of elements in the refined zone.

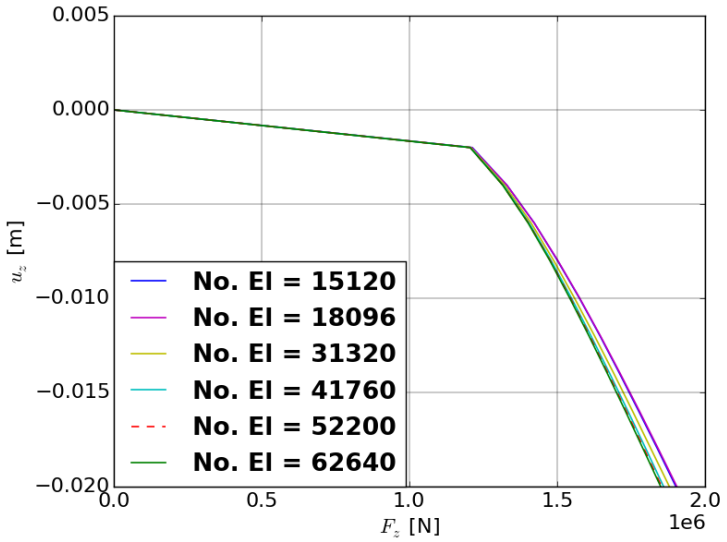

Figure 19: Load-settlement curve for mesh dependency.

5.4 Size of the refined domain

Adopting the same assumptions described in section 5.3, dimensions of the refined domain are now examined. Results are presented in Figure 20, where it can be seen that for $\alpha = 1.5D$ (D : Diameter) we have the minimum size of the refined domain and thus the minimum problem in terms of finite elements. Even if this value seems ideal for the computation, a value of $\alpha = 2D$ was chosen. This choice was based on the computational time of the numerical analysis. A total time of 9 minutes was needed for $\alpha = 2D$, instead of 33 minutes for $\alpha = 1.5D$. This is due to the fact that non linearities still appear in a distance greater than $1.5D$ at the base of the pile, and thus the larger elements at the interface between the refined and not refined domains, impose an increase of iterations (= increase of computational time) before attaining equilibrium.

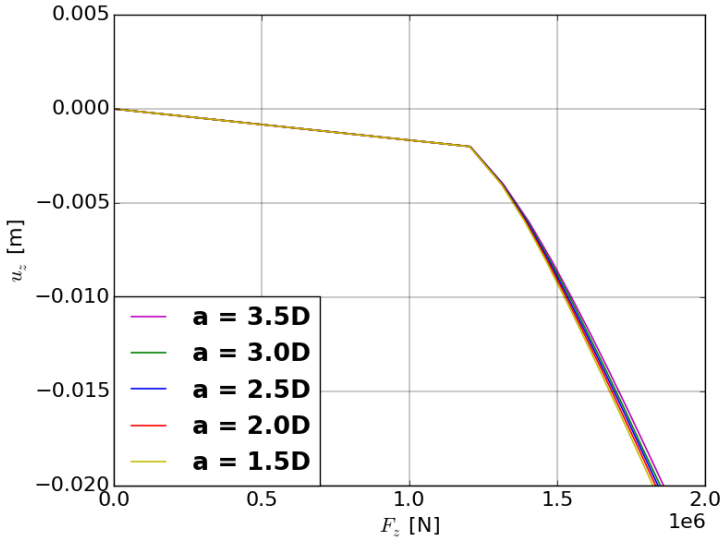

Figure 20: Dimensions of the refined domain.

5.5 Influence of numerical parameters K_N, K_T, and K

A sensitivity study on numerical parameters of the model allows better understanding of the model behavior. Supposing fixed values for other parameters (Table 4) a variation of $K_N = K_T$ is examined, followed by a variation of K. Results are presented in Figure 21a and 21b respectively.

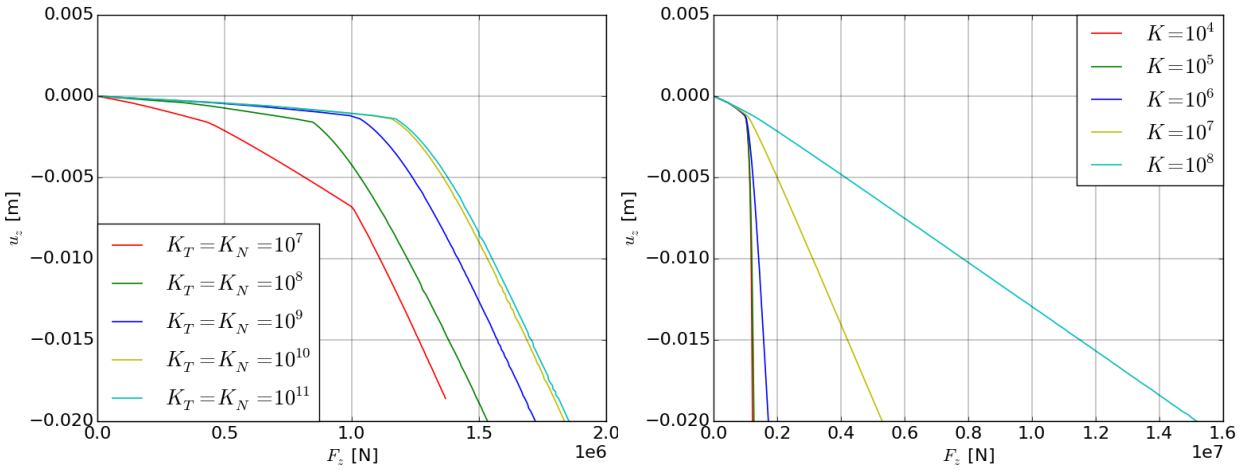

(a) Load-settlement for K_N, and K_T variation. (b) Load-settlement for variation of K.

Figure 21: Sensitivity of numerical parameters of joint elements (K_N, K_T, and K).

As expected, an increase in K_N and K_T increases the stiffness of the model, and an impact is observed in the first part of the curve. In the same way, an increase in K increases the slope after yielding and thus the second part of the curve is influenced. A concluding remark deriving from Figure 21, is that for values of $K_N = K_T \geq 10^{10}$ and $K \leq 10^5$ allows to obtain a stabilized global response.

5.6 Influence of physical parameters μ and c

Physical parameters of the interface, μ, and c influence the capacity in lateral friction. This can be observed from numerical results Figures 22a, and 22b where an increase in μ, or c causes an increase in the yielding limit of the pile soil-interface.

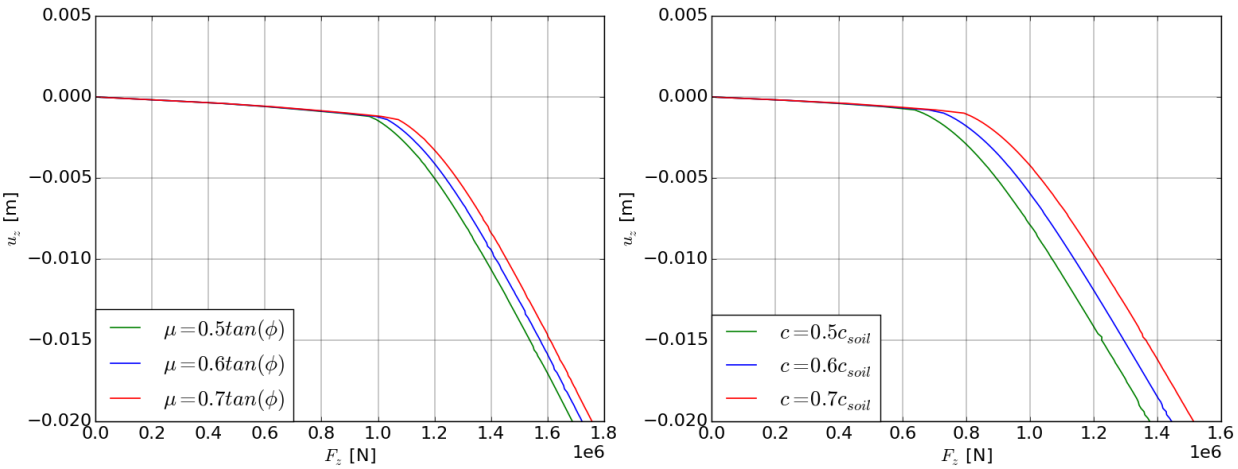

(a) Impact of friction angle coefficient μ. (b) Impact of cohesion c.

Figure 22: Influence of physical parameters of joint elements (μ, and c).

5.7 Influence of initial stress field (K_0)

As previously explained (section 4.3) initial stress field in soil is defined using the Jacky's rule (equation 4.6). Here, even though the case study supposes a bored pile, an extreme value of $K_0 = 1$ is chosen so as to evaluate the impact on system response. Results are presented in Figure 23, where an an important difference can be observed in yielding force which is the value taken into account when in pile design.

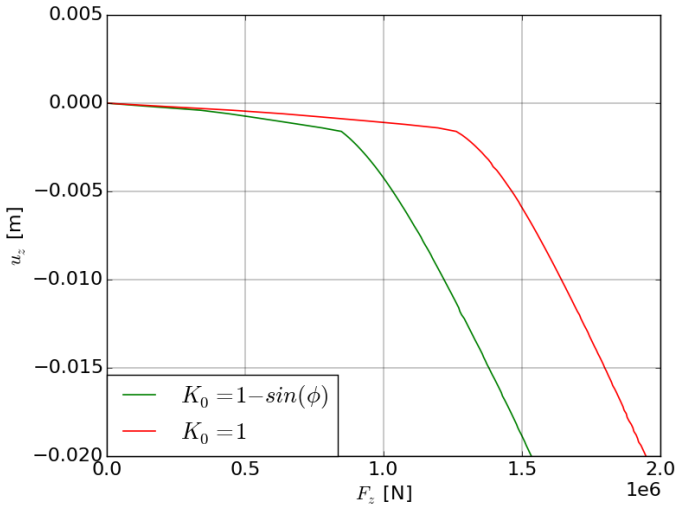

Figure 23: Load-settlement curve for a variation of K_0.

5.8 Calibration of interface and soil parameters

Mechanical characteristics presented in Table 4 are adopted in this section. Values concerning Young's Modulus E_s, friction angle ϕ, unit weight γ, and earth pressure coefficient K_0 are not modified. Calibration procedure explained in section 4.5 is adopted.

- Case 1 : Numerical parameters of joint elements
  Model calibration is carried for numerical parameters of joint elements K_N, K_T, and K. As previously discussed (section 5.5) for increased values of $K_N = K_T$ global response is independent of those values. Subsequently, the minimum (better condition number of the matrix) of all stabilization values is searched at first. A final calibration of K provides the slope of the second part of the curve.

- Case 2 : Parameters of joint elements and soil cohesion
  Values of $K_N = K_T$ are fixed so as to not influence global response. Friction angle coefficient is fixed in it's maximum value of $\mu = 0.7 \times \tan\phi$, and adhesion of joint elements is taken as $c = c_{soil}$. Friction angle and cohesion of soil are chosen next so as to obtain the yielding limit of the curve and in the end the value of K is defined so as to adjust the slope of the second part of the curve.

Table 5 assembles the final numerical values according to the aforementioned procedure.

		$K_N = K_T$ [GPa]	K [MPa]	c [kPa]	μ	ϕ	c_{soil} [kPa]
Very Stiff Clay	Case 1	10	8	c_{soil}	$0.7 \times \tan\phi$	20	13
Sand			2			34	0.1
Very Stiff Clay			15			26.5	57
Shale			15			26	70
Very Stiff Clay	Case 2	10	2	c_{soil}	$0.7 \times \tan\phi$	25	26
Sand			0.5			34	5
Very Stiff Clay			0.5			28	70
Shale			26			28	70

Table 5: Parameters of the numerical model.

Along with the aforementioned calibration cases, numerical analyses where linear behavior or non-linearities of each separate element were examined (lateral friction, or end-bearing capacity). All numerical results are assembled in Figure 24.

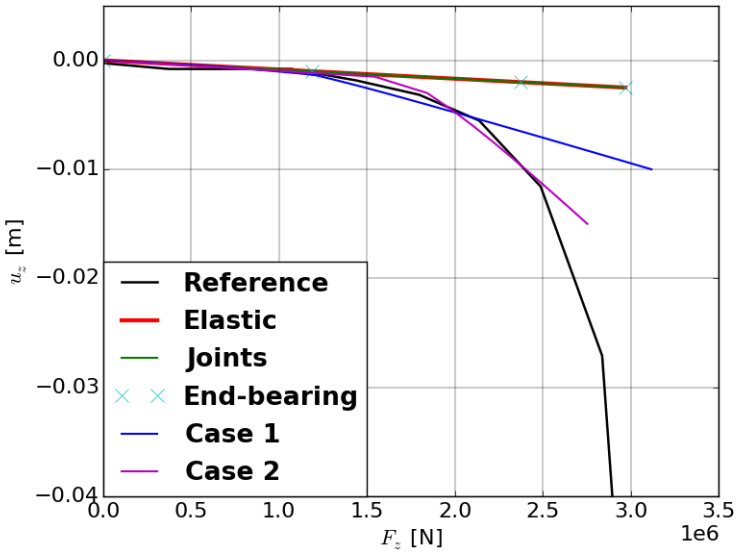

Figure 24: Calibration of the model.

Main observations of the numerical analysis are listed below :

- Elastic behavior overestimates pile capacity and results do not correspond to reality;
- Lateral friction, or bearing capacity when considered uncoupled, and for the values of final model calibration reproduce the behavior of the elastic model. This is related to the fact that global response is rigid, and thus displacements that mobilize friction or activate plastic deformation at the pile base cannot be developed ;

- When both failure mechanisms are taken into account, the model is better capable of approximating experimental results. Case 1, produces a good approximation of the first part of experimental curve, while with the calibration of physical parameters in Case 2 a better global approximation is provided up to 1 cm. Given the fact that most of the time the critical parameter for pile design is the "tolerated" level of displacements, we conclude that numerical results are satisfactory for the estimation of pile-soil interaction under an axial load.

Before concluding with this numerical analysis a representation of the vertical stress field as well as the plastic zone in soil are presented in Figures 25a, and 25b. Considering the plastic zone a similar form with the one proposed from Skempton [1951] in Figure 5 can be observed.

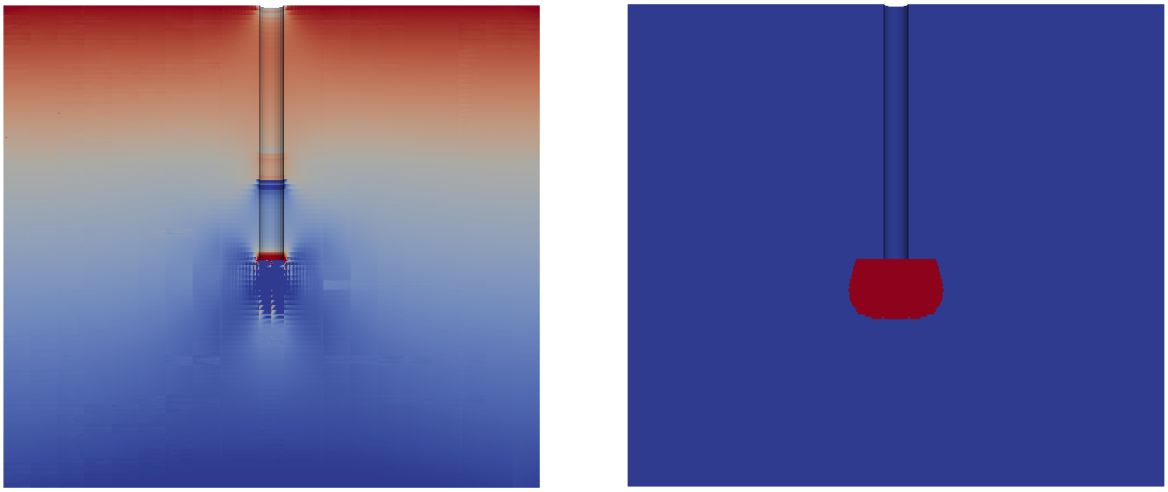

(a) Vertical stress σ_{zz} in soil.

(b) Plastic zone in soil.

Figure 25: Stress and plastic zone in soil.

5.9 Concluding remarks

The present chapter provides an overview of important aspects regarding pile-soil interaction under axial load.

An essential step of modelling procedure is the estimation of mechanical characteristics of soil which is provided through correlation with experimental results. An important uncertainty derives from this step which is crucial for the correct estimation pile-soil interaction.

It arises from the presented study that the coupling of both non-linear phenomena (lateral friction, end-bearing soil behavior) allows a satisfactory estimation of the global response of the system, while the elastic model or each of the separate mechanisms overestimate pile-soil response.

Nevertheless, an important drawback of the model is the existence of numerical parameters for joint elements. Calibration is strongly influenced from these parameters which are changed so as to obtain experimental curve. When in real cases of pile-soil interaction, experimental curves have to be used so as to calibrate numerical parameters. However, this calibration consists for the problem another source of uncertainty and thus the development of a more "physical" model for joint elements is necessary.

A concluding remark refers to the way that we impose external load. Imposed displacements were chosen in this analysis so as to facilitate convergence with the Mohr-Coulomb criterion. A discussion concerning this choice is provided in the following chapter where the response of single piles under lateral monotone loading is examined.

6 Pile response to lateral monotone loading

This case consists of an intermediate step before continuing to the lateral cyclic loading. It is presented here so as to complete the case of monotone loading and even though, numerical results are not compared to experimental ones this step is necessary so as to better understand model behavior for a lateral loading.

We adopt the same geometry and mechanical characteristics described in the previous case and a lateral load of 30MN is applied at the head of the pile so as to investigate the system response. Soil media around the pile are now modeled using the Mohr-Coulomb criterion while soil at the base of the pile is supposed to be elastic (see Figure 17b). Joint elements represent the pile-soil interface.

6.1 Soil behavior to lateral monotone loading

We are interested in generating the $p-y$ curve for the soil (see also Chapter 2.3.3.1). Data are measured on the first point between joints and soil and with respect to the depth (blue cross in Figure 29). The value of p is computed as the product of the diameter D with the equivalent Von Mises stress defined from equation 6.1.

$$\sigma_{VM} = \sqrt{\frac{3}{2} s_{ij} s_{ij}}, \text{ where } s_{ij} = \sigma_{ij} - \frac{1}{3} tr(\sigma)\delta_{ij} \tag{6.1}$$

where s_{ij} is the deviatoric stress tensor and δ_{ij} is the identity matrix. Displacement y in the direction of the force is also taken at the same points. Figure 26, assembles the $p-y$ curves for different depths from the surface.

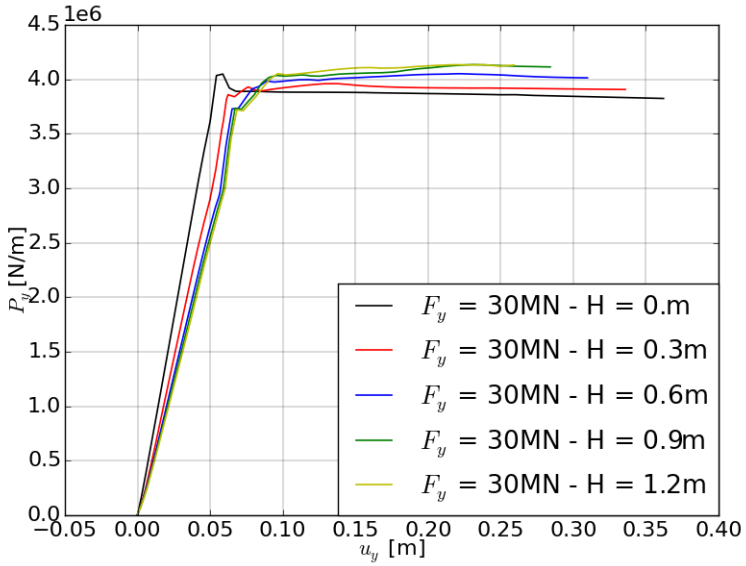

Figure 26: Soil pressure curve.

According to this Figure 26, $p-y$ curve correspond to the ones of an elastic-perfectly plastic soil as described in the literature and Eurocodes (AFNOR [2012]). Main conclusions referring to Figure 26 are :

- With an increase of depth an increase in soil capacity is observed (difference between yellow and blue line).

- Free surface soil (black line) seems to have a softening behavior, which is related to the free border effect. As we advance in depth we come across to the expected elasto-plastic behavior.
- Numerical analysis adopting the Mohr-Coulomb criterion with imposed force, may lead to convergence problems due to the non existence of solution for the case of an applied load that surpasses the limit load. As a result, given the fact that we search to model until failure, numerical analysis with Mohr-Coulomb are to be conducted on imposed displacements when this is possible.

When σ_{yy} stress distribution is examined (Figure 27), a compression area is observed at the front of the pile above rotation center and at the back of the pile below rotation center (blue color in Figure 27a). Traction (red zone) appears at the opposite sides of compression. Higher values of traction are observed at the lateral side of the pile on an angle perpendicular to the load, where pile-soil friction takes place.

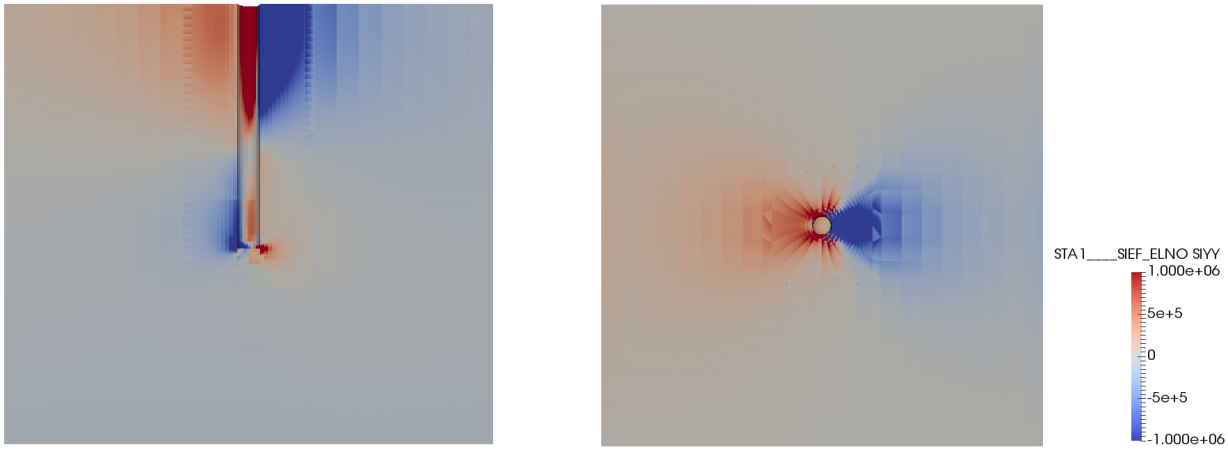

(a) Stresses σ_{yy} (cut at pile center). (b) Stresses σ_{yy} (view of the top of the pile).

Figure 27: Stresses σ_{yy} in soil.

Considering plastic deformation on soil, the internal variable $V3$ for the Mohr-Coulomb criterion allows to identify the plastic region. For $V3 = 1$ a plastic state is established, while for $V3 = 0$ soil behaves elastically. Figure 28 represents a $z - y$ plane cut view in the middle of the pile and the values of $V3$ are plotted for soil media.

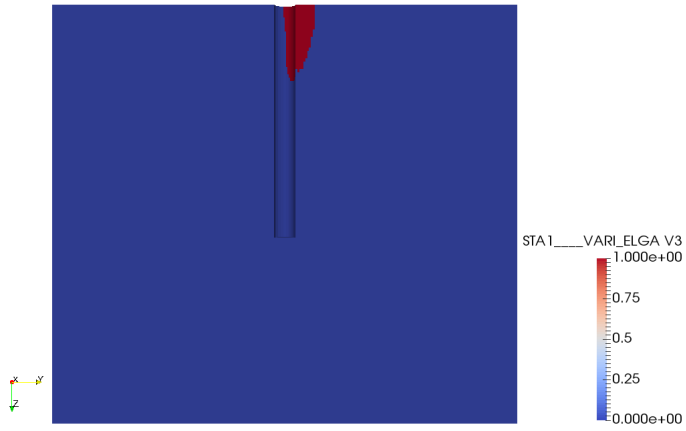

Figure 28: Internal variable of plastic deformation (plastic = 1, elastic = 0).

As we can see, soil creates a plastic zone in a form of a wedge at the front of the pile in the direction of loading.

6.2 Joint behavior to lateral monotone loading

Internal variables of joints are examined here, so as to verify sliding (internal variable $V2$) and opening (internal variable $V5$) of the joints. When joints are open (or when in plastic region for sliding) the internal variable takes the value 1, while for a closed joint (or when in elastic region for sliding) a value of 0 is given. Values of internal variables are measured in the front of the pile for opening (blue cross in Figure 29), and, at the lateral to the load side for sliding (red cross in Figure 29).

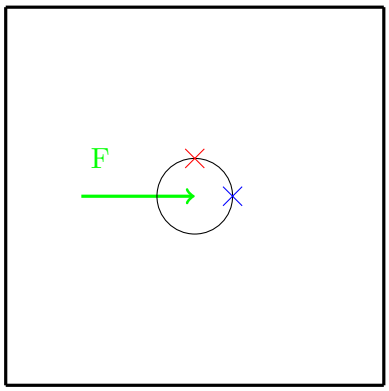

Figure 29: Points where internal variables are measured (sliding=red, opening=blue).

Figure 30b represents the evolution of $V5$ with time and for different points in pile profile. In parallel to these internal variables the profile of displacement for the pile is plotted in Figure 30a. Main remarks from Figure 30 are :

- In accordance to Figure 27a, pile is divided in two parts : 1) an upper part where soil is compressed (joints are closed $V5 = 0$), and; 2) a lower part where traction takes place (joints are open $V5 = 1$). The change point between the two states is the rotation center of the pile.
- With the increase of external load a progressive shift of the rotation center towards the surface takes place. According to Figure 30b, a load $F_y \geq 13.2$ MN results in the stabilization of the rotation center at a depth $H \approx 5.8$m, while for a lower external value $F_y = 5.4$MN rotation center was at $H \approx 7.9$m.

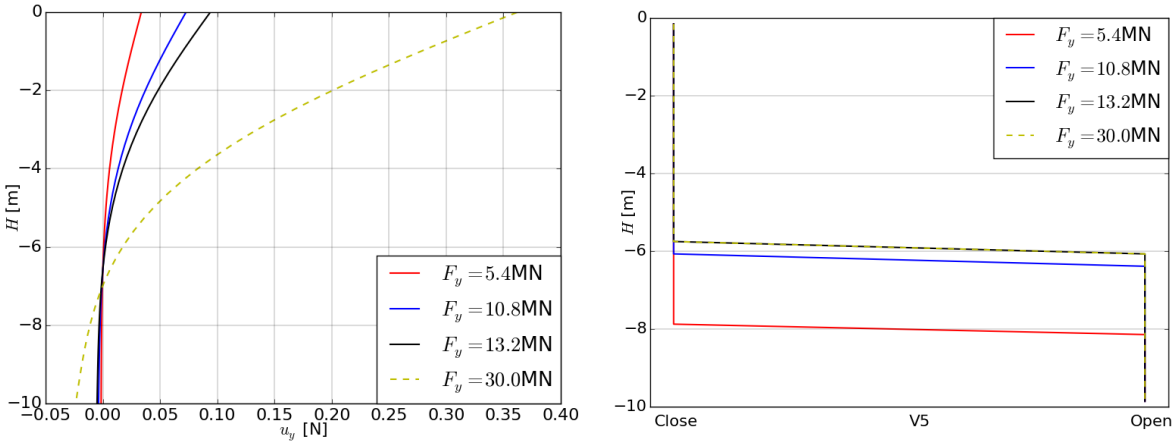

(a) Deflection with depth.

(b) Internal variable of opening $V5$.

Figure 30: Numerical results with respect to pile profile.

Sliding is examined through the evolution of internal variable $V2$ with depth and results are given on Figure 31. Different levels of load are examined so as to better visualize the

evolution of internal variables, and it can be observed that joint elements slide progressively with the increase of the applied load. For a value $F_y \geq 6$MN the pile has moved horizontally sufficiently enough so as to mobilize friction to all of it's nodes.

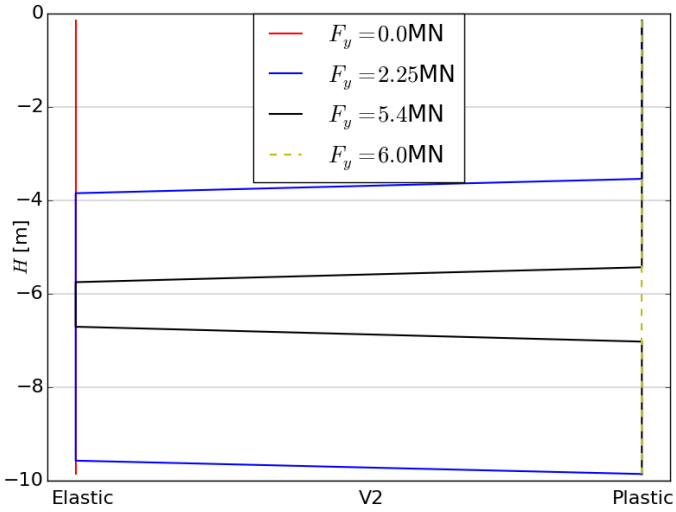

Figure 31: Evolution of internal variable of sliding $V2$.

6.3 Concluding remarks

The present chapter provides an overview of important aspects regarding lateral monotone loading of pile foundations. Analysis focuses on the study of internal variables of soil and joint elements, as well as the stress field of soil.

Lateral soil behavior corresponds to the elastic-perfectly plastic behavior described in Eurocodes, and used in the framework of load-transfer method. A possible source of numerical problems was found for the Mohr-Coulomb criterion when external load is considered in terms of imposed forces. Stresses in the direction of loading are consistent with the load and verify the passive earth pressure profile for short piles proposed in Eurocodes (see AFNOR [2012]). The creation of a plastic zone in the form of wedge is also in correspondence with the theory of Broms [1964a] for short piles in cohesive soils.

The aforementioned were justified from the study of internal variables in joint elements. Variables of sliding and opening of the joint were examined and results show a coherence with the stress field in the soil and the profile of pile displacement. This study concludes the analysis of lateral load in joint elements and in the next chapter cyclic behavior is to be examined.

7 Pile response to lateral cyclic loading

The reference case consist of an experimental campaign conducted by Jennings et al. [1984] and studies the behavior of bored cylindrical piles under cyclic lateral loading.

7.1 Case study description

A cylindrical bored pile is supposed for this case study. The pile consists of an exterior steel pipe, of a diameter $D = 0.45$m (wall thickness 10mm), initially installed in place and then filled with reinforced concrete. It's length is equal to $L = 8.1$m, and the given mechanical characteristics for concrete and steel are $E_c = 26$GPa and $E_s = 200$GPa, respectively. Poisson ratio is supposed $\nu_c = \nu_s = 0.2$. The geometry of the problem is given in Figure 32a, while in Figure 32b the results of an SPT test on the profile of the pile are presented (east pile). Those experimental results allow the estimation of important parameters for mechanical characteristics of soil through correlation with existing curves.

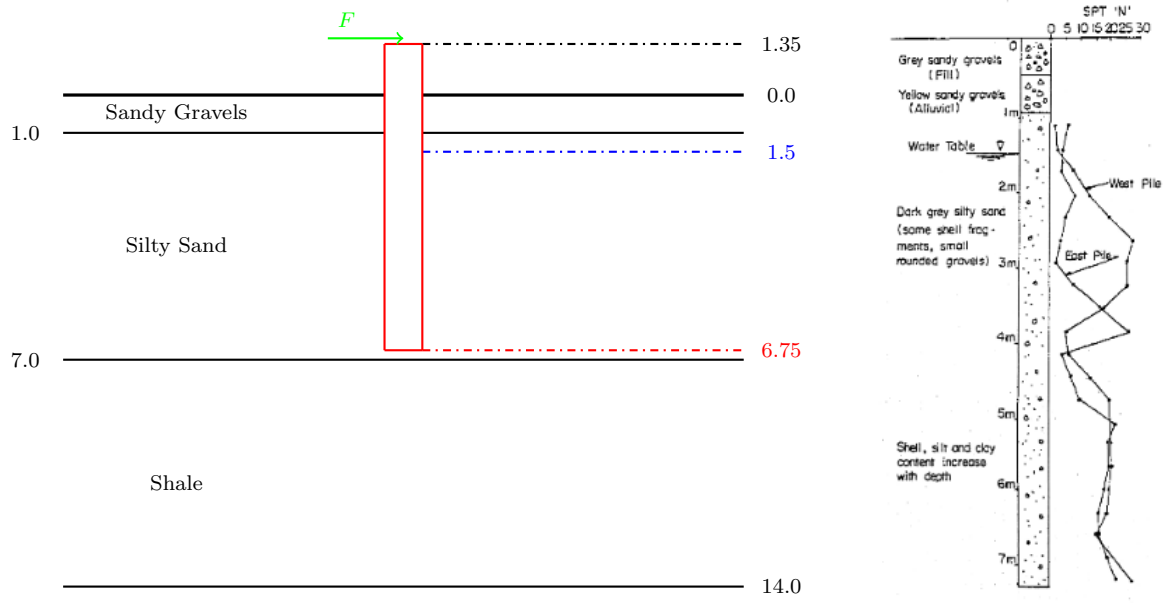

(a) Geometry of the domain (b) SPT 'N' profile

Figure 32: Lateral cyclic loading of bored piles (Jennings et al. [1984])

Considering loading conditions, a lateral cyclic load is applied at the head of the pile in the following sequence : 10kN, 20kN, 40kN (two cycles), 80kN (two cycles), 120kN (two cycles), 160kN (two cycles), 200kN (two cycles), and the displacement of the pile is measured at ground level. Water level is at 1.5m from ground surface.

7.2 Definition of mechanical properties

Friction angles for soil were defined from correlation with SPT curves where the angle is obtained according to the SPT 'N' value (east pile in Figure 32b) and the effective vertical stress (Hunt [2005]). For initial soil layers the static cone resistance q_c is given (Table 6) and thus the estimation of Young's Modulus is computed according to equation 4.1 and values obtained from Tables 2 and 3 (section 4.2). For layers where no q_c data are provided values of shear modulus for small strains are obtained from Hunt [2005]. Young's Modulus is then estimated through equation 7.1, where $\nu = 0.3$ for the soil :

$$E = 2(1 + \nu) \times G \tag{7.1}$$

Indicative values of unit weight are taken from Hunt [2005] according to soil type. Numerical data are presented in Table 6.

Zone	Depth [m]	q_c [MPa]	E [MPa]	γ [kN/m^3]	ϕ	K_0
1	0.5	-	90	18.9	28	0.53
2	1.0	4.5	90	18.9	28	0.53
3	1.5	2.	50	20	29	0.51
4	3.0	7.5	110	20	27	0.54
5	4.0	-	120	20	23	0.61
6	5.0	-	125	20.6	25	0.58
7	7.0	-	180	20.6	26	0.56
8	15.0	-	200	20.6	28	0.53

Table 6: Initial values for mechanical properties of soil.

No information are provided concerning the percentage of steel reinforcement in the pile and thus a hypothesis is made, and an equivalent Young's Modulus is obtained through equation 7.2:

$$E_{pile} = \frac{E_c \times A_c + E_s \times A_s}{A_c + A_s} \tag{7.2}$$

where A_c and A_s is concrete and steel area respectively. A value of $E_{pile} = 56$MPa is fixed.

The provided experimental results are the load-deflection curve, as well as deflection and moment profile of the pile for the following level of load : 40kN, 120kN, and 200kN.

7.3 Calibration of interface and soil parameters

Soil parameters are adopted from Table 6. Friction angle coefficient is defined as $\mu = 0.6 \times \tan\phi$. Joint adhesion is calibrated so as to allow opening of pile-soil interface in the pile area situated behind the direction of loading, where numerical problems related to soil traction may appear. For all the conducted simulations a value of $c = 100$Pa was adopted. Numerical parameters of joints are calibrated so as to approximate the experimental displacement profile. More precisely, an initial analysis supposes only the first cycles of loading (until 120kN). An important remark deriving from numerical simulations is that a high ratio between $K_N = K_T$, with Young's modulus for soil, or between K and $K_N = K_T$ consist a source of possible numerical problems. Two constitutive behaviors were examined for lateral soil, while soil below pile base is supposed elastic (see also Figure 17).

1. Iwan's Law
   An initial estimation of model parameters n and γ_{ref} is obtained through correlation with existing $G - \gamma$ curves from the literature. The $G - \gamma$ curve proposed by Seed and Idriss [1971] was adopted in this work. A final calibration of those parameters is obtained so as to better approximate experimental results.

2. Mohr-Coulomb's criterion
   Friction angle for soil is fixed according to Table 6, and is equal to the dilatancy angle. Soil cohesion is calibrated at $c = 50$kPa for all soil layers. The choice of this value is principally based in numerical problems when lower values were adopted for soil. As previously discussed in section 6.1, when Mohr-Coulomb criterion is adopted for modelling of soil behavior, along with imposed displacements a difficulty in convergence was observed.

Table 7 assembles the final numerical values according to the aforementioned procedure.

Constitutive Model	$K_N = K_T$ [MPa]	K [kPa]	c [Pa]	μ	c_{soil} [kPa]	γ_{ref}	n
Mohr-Coulomb	10	10	100	$0.6\times \tan\phi$	50	-	-
Iwan					-	4.5×10^{-4}	0.76

Table 7: Parameters of the numerical model.

A comparison of numerical results adopting the two constitutive models is presented on Figure 33.

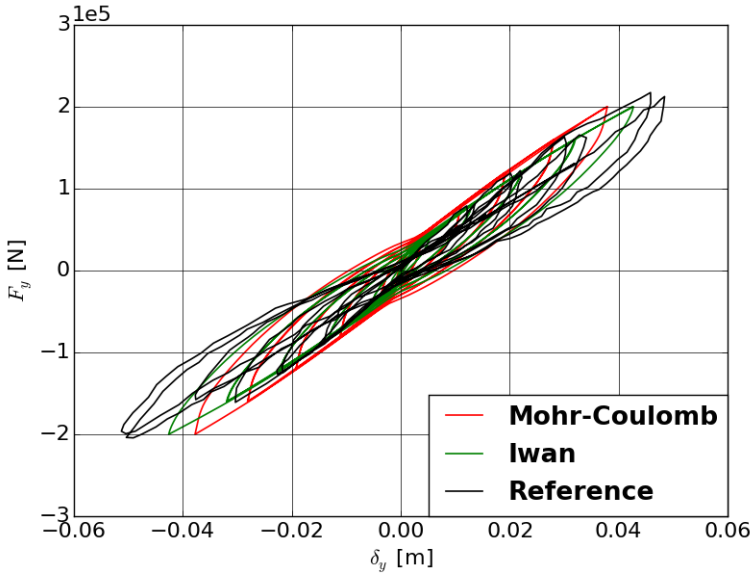

Figure 33: Load-deflection curve.

Both models efficiently describe pile-soil behavior, while the Mohr-Coulomb criterion presents a more rigid behavior than Iwan's law. This is related to the elevated value of soil cohesion that was chosen for the soil and the choice of which was more related to numerical reasons than physical description of the problem. The deflection as well as the moment profile for the pile are given in Figures 34 and 35 respectively.

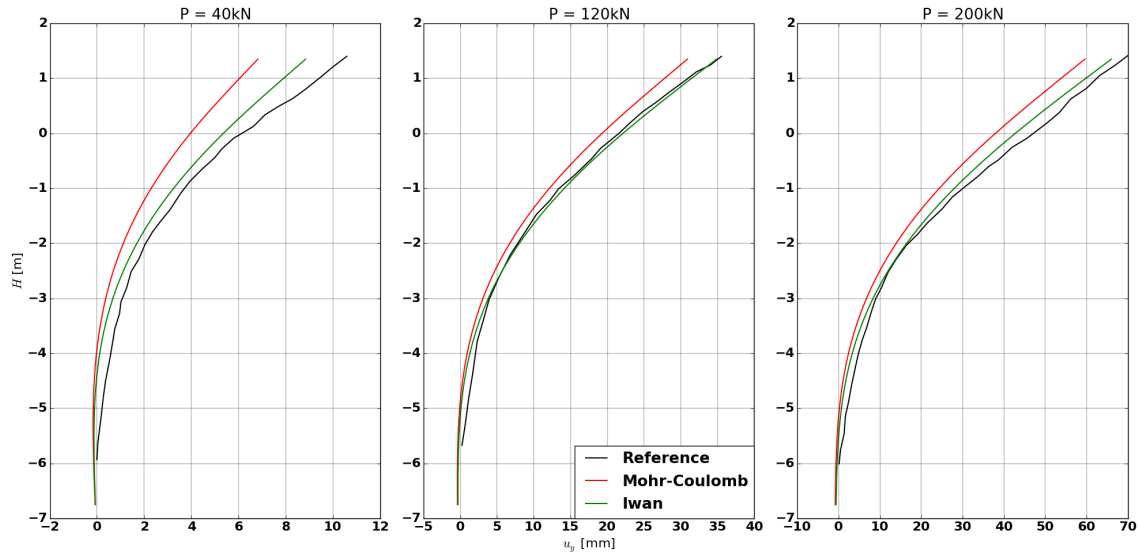

Figure 34: Lateral deflection profile with respect to the applied load.

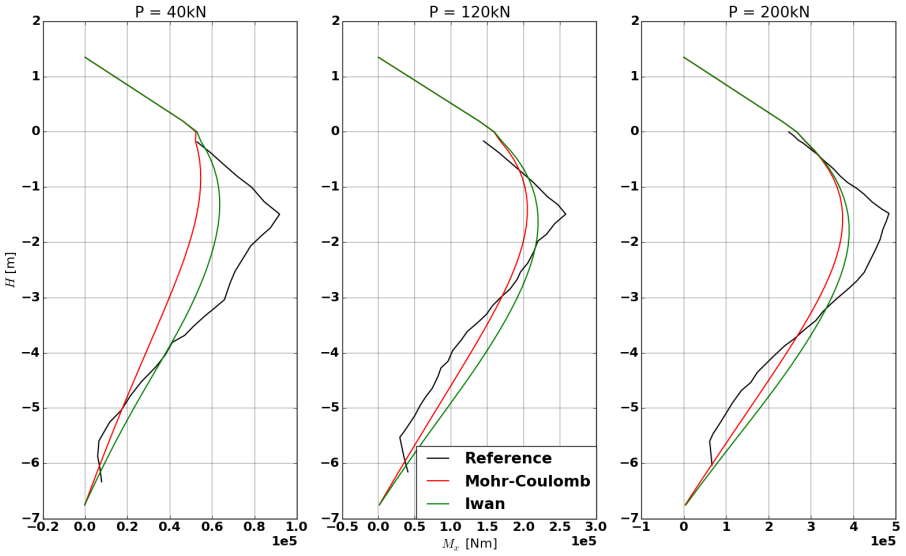

Figure 35: Moment profile with respect to the applied load

Both numerical models provide a good approximation of experimental results. The more rigid behavior of Mohr-Coulomb is also observed in the estimation of lateral deflection and moment profile for the pile. Numerical results with Iwan's law provide a very close approximation of deflection and moment profile especially for more elevated values of external load.

7.4 Concluding remarks

The present chapter provides an overview of important aspects regarding lateral cyclic loading of pile foundation. Numerical results were compared to experimental ones, and main conclusions are presented below.

Physical and numerical parameters of joint elements have been calibrated so as to allow pile-soil detachment and avoid unwanted numerical problems. A low value of adhesion was imposed so as to instantaneously open joints in traction. This consists of an important drawback of joint elements, as the same value of adhesion is also used in the estimation of friction capacity (ϕ and c in the Mohr-Coulomb criterion). A short term solution would be to create zones of joint elements where behavior of the joint is controlled according to the type of stress field exerted in joints, while a long term and more efficient solution would be to change the constitutive law so as to uncouple both phenomena or even directly suppose that traction capacity is equal to zero for the joint (Mohr-Coulomb criterion with tension cut-off).

It arises from numerical simulations that pile-soil response is strongly related to numerical values of $K_N = K_T$ and K. This consists of a contradiction when compared to the axial case, where the value of $K_N = K_T$ was fixed so as not to influence numerical results, and it increases the difficulties of parameters calibration for the case of a multidimensional loading deriving for example from a dynamic analysis of the same pile-soil system.

Both numerical models tested here provide a good approximation of experimental results. From a computational point of view, Iwan's law is by far more adapted for cyclic loading. As an indicative example we simply cite here that numerical simulations with Iwan's law lasted about 13 hours, while for the Mohr-Coulomb criterion computational time went up to 27 hours.

8 Conclusion and Perspectives

Theoretical aspects as well as a numerical modelling strategy for pile-soil interaction were discussed in the present work. A full-FEM 3D model with joint elements and nonlinear soil behavior was presented and tested under axial and lateral monotone as well as lateral cyclic loading. Concluding remarks were already provided throughout this work, and thus only main conclusions are going to be discussed here.

Estimation of bearing capacity for pile-soil interaction remains a complex task related to the strongly non-linear behavior of friction interface and lateral or end-bearing soil. The uncertainties in the estimation of soil-pile response are usually high as it depends on the evaluation of both mechanical characteristics of soil and pile-soil interface.

The proposed numerical model allows the estimation of global response for the examined external loads. Yet, a strong dependence on numerical parameters of joints was observed. In actual cases experimental curves from the site of interest have to be used so as to *a priori* calibrate numerical parameters. This calibration consists from it's own a supplementary source of uncertainties and thus a more "physical" model for pile-soil interface is necessary in order to better approximate pile-soil behavior.

Moreover, in the present version of joint elements, elastic behavior is adopted for the normal component (opening). A more elaborated model where elasto-plasticity or fracture mechanics are imposed in both directions can better represent real behavior of the interface and is more adapted for studies where dynamic load is applied. It is in these cases that the external load "activates" both tangential and normal components of joint plasticity.

Difficulties in convergence of numerical model were observed when imposed forces were adopted for the application of external load and a Mohr-Coulomb criterion represented constitutive behavior of lateral or end-bearing soil. Imposed displacements were applied in certain numerical analysis of this work in order to facilitate convergence. Nevertheless, in actual cases most of the time external loads are known in terms of forces and thus displacements have to be estimated.

Following the analysis, and main conclusions deriving from this work, a series of recommendations for future studies are provided with the following.

A multi-fibre representation of pile can provide a more accurate representation of pile in terms of resistance and mechanical characteristics of the cross-section. For a lateral load, the case of long piles can be examined where pile plasticity is taken into account and thus pile-soil failure mechanism is similar to the one described in Figure 11b;

The proposed model was able to properly represent experimental results for lateral cyclic loading. Yet, dynamic loading has to be examined so as to evaluate limitations and validate the aforementioned discussion concerning numerical parameters of joints.

In everyday engineering applications, single piles are seldom to be found. On the contrary, group of piles are used so as to assure stability of the superstructure. Theoretical studies have yet to be conducted so as to investigate critical aspects of failure for a group of piles. Numerical modelling will allow a better understanding of this challenging issue. Group effect's phenomena have to be examined and results have to be compared to actual cases so as to validate the possible proposed numerical strategies.

A final goal would be the analysis of an actual case of soil-structure interaction. A modelling strategy has to be developed for a model validation with actual case studies. A further comparison with other numerical procedures proposed in the literature (section 2.3.3) can pinpoint the importance and utility of the proposed model.

References

code_aster. General public licensed structural mechanics finite element software. http://www.code-aster.org. Accessed: 2018-08-08.

Harry George Poulos. Pile behaviour—theory and application. *Geotechnique*, 39(3):365–415, 1989.

Maurice Cassan. Les essais in situ en mécanique des sols. Technical report, Eyrolles, 1988.

Vinicius Alves Fernandes. *Numerical analysis of nonlinear soil behavior and heterogeneity effects on railway track response*. PhD thesis, Ecole Centrale Paris, 2014.

KM Chua. Determination of cbr and elastic modulus of soils using a portable pavement dynamic cone penetrometer. In *Penetration testing*, pages 407–414, 1988.

RP API. 2geo (2011) geotechnical and foundation design considerations. *American Petroleum Institute, Washington, DC, USA Google Scholar*, 2011.

R7.01.28. Loi de Mohr-Coulomb, Document de référence R7.01.28 de Code_Aster, 2016. URL https://www.code-aster.org/V2/doc/v14/fr/man_r/r7/r7.01.28.pdf.

Karl Terzaghi, Ralph B Peck, and Gholamreza Mesri. *Soil Mechanics in Engineering Practice Third Edition*. 1996. ISBN 0471086584 9780471086581. doi: 10.1016/S0013-7952(97)81919-9.

V Shakhirev, JP Magnan, and H Ejjaaouani. Etude expérimentale du comportement du sol lors du fonçage des pieux. *Bulletin-Laboratoires Des Ponts Et Chaussees*, pages 95–116, 1996. URL http://www.geotech-fr.org/sites/default/files/revues/blpc/BLPC206pp95-116Shakhirev.pdf.

FC Chow. Investigations into displacement pile behaviour for offshore foundations. *Ph. D Thesis, Univ. of London (Imperial College)*, 1997.

Sofia Costa Aguiar. *Numerical modelling of soil-pile axial load transfer mechanisms in granular soils*. PhD thesis, ECOLE CENTRALE PARIS, 2008.

MF Randolph. Design consideration for offshore piles. In *Proc. Conf. on Goet, Practice in Offshore Engrg. Div., ASCE*, pages 422–439, 1983.

Ken Fleming, Austin Weltman, Mark Randolph, and Keith Elson. *Piling engineering*. Third edition, jul 2008. ISBN 9780203937648.

Jean-Louis Briaud, Marc Ballouz, and George Nasr. Static capacity prediction by dynamic methods for three bored piles. *Journal of Geotechnical and Geoenvironmental Engineering*, 126(7):640–649, 2000.

DN Jennings, SJ Thurston, and FD Edmonds. Static and dynamic lateral loading of two piles. In *Proc 8th WCEE*, pages 561–68, 1984.

Bengt B Broms. Lateral resistance of piles in cohesive soils. *Journal of the Soil Mechanics and Foundations Division*, 90(2):27–64, 1964a.

Roger Frank and Philippe Mestat. Aspects expérimentaux et numériques du frottement latéral des pieux. *Mécanique & industries*, 1(6):651–666, 2000.

Zineb Abchir. *Contribution à l'étude du comportement des pieux soumis à des sollicitations axiales monotones et cycliques*. PhD thesis, Université Paris-Est, 2016. URL https://tel.archives-ouvertes.fr/tel-01459082.

Karl Terzaghi. *Theoretical Soil Mechanics*. John Wiley & Sons, Inc., Hoboken, NJ, USA, jan 1943. ISBN 9780470172766. doi: 10.1002/9780470172766. URL http://doi.wiley.com/10.1002/9780470172766.

R7.01.25. Lois de comportement des joints des barrages : JOINT_MECA_RUPT et JOINT_MECA_FROT, Document de référence R7.01.25 de Code_Aster. 2016. URL https://www.code-aster.org/V2/doc/v10/fr/man_r/r7/r7.01.25.pdf.

Bujang B K Huat. A Review of Basic Soil Constitutive Models for Geotechnical Application. *Electronic Journal of Geotechnical Engineering*, 14, 2009. URL https://www.researchgate.net/publication/228565882.

Poul V. Lade. Overview of Constitutive Models for Soils. *Soil Constitutive Models*, 40771 (January 2005):1–34, 2005. ISSN 08950563. doi: 10.1061/40771(169)1. URL http://ascelibrary.org/doi/abs/10.1061/40771%28169%291.

R7.01.38. Loi d'Iwan pour le comportement cyclique de matériaux granulaires, Document de référence R7.01.38 de Code_Aster, 2017. URL https://www.code-aster.org/doc/default/fr/man_r/r7/r7.01.38.pdf.

L Prandtl. On the penetrating strengths (hardness) of plastic construction materials and the strength of cutting edges. *ZAMM Journal of Applied Mathematics and Mechanics*, 1(1):15–20, 1921.

G G Meyerhof. The Ultimate Bearing Capacity of Foudations. *Géotechnique*, 2(4):301–332, dec 1951. ISSN 0016-8505. doi: 10.1680/geot.1951.2.4.301. URL http://www.icevirtuallibrary.com/doi/10.1680/geot.1951.2.4.301.

Y. M. Cheng. Nq factor for pile foundations by Berezantzev. *Géotechnique*, 54(2):149–150, mar 2004. ISSN 0016-8505. doi: 10.1680/geot.2004.54.2.149. URL http://www.icevirtuallibrary.com/doi/10.1680/geot.2004.54.2.149.

Aleksandar S Vesic. Analysis of ultimate loads of shallow foundations. *Journal of Soil Mechanics & Foundations Div*, 99(sm1), 1973.

HG Poulos and EH Davis. Pile foundation analysis and design. Technical report, John Wiley, 1980.

Michael John Tomlinson and R Boorman. *Foundation design and construction*. Pearson education, 2001.

Imen Said. *Comportement des interfaces et modélisation des pieux sous charge axiale*. PhD thesis, Ecole des Ponts ParisTech, 2006.

Daichao Sheng, K. Dieter Eigenbrod, and Peter Wriggers. Finite element analysis of pile installation using large-slip frictional contact. *Computers and Geotechnics*, 32(1):17–26, 2005. ISSN 0266352X. doi: 10.1016/j.compgeo.2004.10.004.

Luis André Berenguer Todo-Bom. *Numerical modeling of soil-pile interaction considering grain breakage in finite deformations*. PhD thesis, Ecole Centrale Paris, 2014.

AFNOR. Norme NF P94-262, Justifications des fondations profondes, 2012.

Bengt B Broms. Lateral resistance of piles in cohesionless soils. *Journal of the Soil Mechanics and Foundations Division*, 90(3):123–158, 1964b.

LC Reese, WF Van Impe, and RD Holtz. Single piles and pile groups under lateral loading. *Applied Mechanics Reviews*, 55:B9, 2002.

Karl Terzaghi. Evalution of conefficients of subgrade reaction. *Geotechnique*, 5(4):297–326, 1955.

Tiago Gerheim Souza Dias and Adam Bezuijen. Load-transfer method for piles under axial loading and unloading. *Journal of Geotechnical and Geoenvironmental Engineering*, 144 (1):04017096, 2017.

Harry M Coyle and Lymon C Reese. Load transfer for axially loaded piles in clay. *Journal of the Soil Mechanics and Foundations Division*, 92(2):1–26, 1966.

HG Poulos and EH Davis. The settlement behaviour of single axially loaded incompressible piles and piers. *Geotechnique*, 18(3):351–371, 1968.

Benjamin Cerfontaine, Anne-Catherine Dieudonné, Jean-Pol Radu, Frédéric Collin, and Robert Charlier. 3d zero-thickness coupled interface finite element: Formulation and application. *Computers and Geotechnics*, 69:124–140, 2015.

K. G. Sharma and C S Desai. Analysis and Implementation of Thin-Layer Element for Interfaces and Joints. *Journal of Engineering Mechanics*, 118(12):2442–2462, 1992. ISSN 0733-9399. doi: 10.1061/(ASCE)0733-9399(1992)118:12(2442).

P Villard. Modelling of interface problems by the finite element method with considerable displacements. *Computers and Geotechnics*, 19(1):23–45, 1996.

Stéphane Grange, Panagiotis Kotronis, and Jacky Mazars. A macro-element to simulate dynamic soil-structure interaction. *Engineering Structures*, 31(12):3034–3046, 2009.

John Lysmer, Mansour Tabatabaie-Raissi, Freddie Tajirian, Shahriar Vahdani, and Farhang Ostadan. *SASSI: A system for analysis of soil-structure interaction*. 1981.

Salome-Meca. http://www.salome-platform.org/. Accessed: 2018-08-08.

Roy E Hunt. *Geotechnical engineering investigation handbook*. Crc Press, 2005.

Alex W Skempton. The bearing capacity of clays. In *Proc. of Building Research Congress*, volume 1, pages 180–189. ICE, 1951.

Harry Bolton Seed and Izzat M Idriss. Simplified procedure for evaluating soil liquefaction potential. *Journal of Soil Mechanics & Foundations Div*, 1971.

S Burlon, Roger Frank, F Baguelin, J Habert, and S Legrand. Model factor for the bearing capacity of piles from pressuremeter test results–eurocode 7 approach. *Géotechnique*, 64 (7):513–525, 2014.

Appendices

A Theoretical solutions for the estimation of bearing capacity of axially loaded piles

A.1 Correlation with experimental data

The estimation of bearing capacity through correlation with experimental data is one of the most popular methods due to their simplicity in application. Two different methods can be distinguished and are briefly presented here. One can found the complete database in AFNOR [2012].

A.1.1 Pressuremeter test

A.1.1.1 Lateral friction

Lateral friction per unit area is expressed according to Burlon et al. [2014] as :

$$q_s = \alpha_{interface} \times f_{soil}(p_l(z)) \tag{A.1}$$

where $\alpha_{interface}$ is a coefficient depending in the construction mode and type of soil, p_l is the limit pressure measured in the soil, and f_{sol} is a function depending in the type of soil. This function is expressed as :

$$f_{sol}(p_l^*) = (\alpha \times p_l^* + b) \times (1 - e^{c \times p_l^*}) \tag{A.2}$$

Coefficients $\alpha_{interface}$, α, b, and c can be found in AFNOR [2012]. Given the value of equation A.1 the friction resistance of a pile with a diameter D and a length L is defined as:

$$Q_s = \pi D \int_0^L q_s(p_l) dz \tag{A.3}$$

A.1.1.2 End-bearing resistance

End-bearing resistance can be defined as :

$$Q_p = \kappa_p \times p_{le}^* \times A_p \tag{A.4}$$

where A_p is the section of the pile. The limit pressure in the point, p_{le}^* is defined as :

$$p_{le}^* = \frac{1}{b + 3a} \int_{L-b}^{L+3a} p_l^*(z) dz, \text{ where } \begin{cases} a = \max(D/2; 0.5) \\ b = \min(a; h) \end{cases} \tag{A.5}$$

The height h defines the part of the pile that is inside the more resistant soil layer. Coefficient κ_p is the coefficient that defines the end-bearing capacity, which depends on the "effective embedding" of the pile defined as :

$$D_{ef} = \frac{1}{p_{le}^*} \int_{L-h_D}^{L} p_l^*(z) dz, \text{ where } h_D = 10D \tag{A.6}$$

According to this value we obtain :

- $\kappa_p = \kappa_{pmax}$, if $\frac{D_{ef}}{D} > 5$
- $\kappa_p = 1 + (\kappa_{pmax} - 1) \times (D_{ef}/D/5)$, if $\frac{D_{ef}}{D} < 5$

Finally, the value of κ_{pmax} which depends to soil type and installation mode, is obtained through tables AFNOR [2012].

A.1.2 Penetration test (CPT)

The estimation of lateral friction and end-bearing capacity with the penetration test is given through the same equations presented for the pressuremeter test. Two main differences can be distinguished between the two methods :

- The expressions are not formed in terms of limit pressure p_l, but in terms of cone resistance q_c. This is related to the way that each method estimates soil capacity.
- For the case of end-bearing capacity, the final expressions of κ_c are now different according to each type of soil. :
  - $\kappa_c = \kappa_{cmax}$, if $\frac{D_{ef}}{D} > 5$
  - if $\frac{D_{ef}}{D} < 5$:
    - $k_c = 0.3 + (k_{cmax} - 0.3)(D_{ef}/D)/5$, for clays
    - $kc = 0.2 + (k_{cmax} - 0.2)(D_{ef}/D)/5$, for intermediate soils
    - $kc = 0.1 + (k_{cmax} - 0.1)(D_{ef}/D)/5$, for sands and gravels
    - $kc = 0.15 + (k_{cmax} - 0.15)(D_{ef}/D)/5$, for marls or fragmented rocks

A.2 Total stress α method

Computational method for the calculation of axial capacity in clays. Installation method is taken into account through the α coefficient.

A.2.1 Lateral Friction

The proposed expression by the API [2011] for the estimation of lateral friction is given by :

$$q_s = \alpha \times c_u \tag{A.7}$$

Where c_u is the undrained shear strength of soil and α is a coefficient given by :

$$\begin{aligned} \alpha &= 0.5 \left(\frac{c_u}{\sigma'_v}\right)^{-0.5}, \text{ if } \left(\frac{c_u}{\sigma'_v}\right) \leq 1 \\ \alpha &= 0.5 \left(\frac{c_u}{\sigma'_v}\right)^{-0.25}, \text{ if } \left(\frac{c_u}{\sigma'_v}\right) > 1 \end{aligned} \tag{A.8}$$

where σ'_v is the vertical effective stress.

A.2.2 End-bearing Capacity

For the end-bearing capacity, the API [2011] proposes :

$$q_p = 9 \times c_u \tag{A.9}$$

A.3 Effective stress β method

A.3.1 Lateral Friction

The estimation of lateral capacity takes into consideration the Mohr-Coulomb criterion (equation 2.1) and the estimation of lateral friction is given as :

$$q_s = \sigma'_h \times \tan(\delta') = K \times \tan(\delta') \times \sigma'_v = \beta \times \sigma'_v \tag{A.10}$$

where K is the earth pressure coefficient for the soil, and δ' is the friction angle of the pile-soil interface. The method proposes a different β coefficient according to the type of soil and construction mode.

For driven piles in sand with an open sections the values of β are given in Table 8, while for the case of a close section an increase of 25% for the given parameters is recommended and according to API [2011].

Relative Density	**Soil Descritpion**	**Shaft Friction factor β**	**Limiting shaft friction values [kPa]**	**End bearing factor N_q**	**Limiting end bearing values [kPa]**
Very Loose Loose Loose Medium Dense Dense	Sand Sand Sand-Silt Silt Silt	Not Applicable	Not Applicable	Not Applicable	Not Applicable
Medium Dense	Sand-Silt	0.29	67	12	3000
Medium Dense Dense	Sand Sand-Silt	0.37	81	20	5000
Dense Very Dense	Sand Sand-Silt	0.46	96	40	10000
Very Dense	Sand	0.56	115	50	12000

Table 8: Design parameters for a cohesionless soil (API [2011]).

For the case of clays, the estimation of β is given through empirical expressions that propose a relation between the β parameter and the internal friction angle of the soil ϕ, as well as the over-consolidation ratio OCR. More precisely, according to Meyerhoff (1976) we can estimate β as :

$$\beta = (1.5 \pm 0.5) \times K \times \delta' \times \sqrt{OCR} \tag{A.11}$$

Different variations of the aforementioned expression have been proposed in the literature (Abchir [2016]), which try to better adapt the estimation of β to specific conditions (construction mode, type of pile).

A correct estimation of β can provide a satisfactory estimation of friction capacity. However, the β parameter tries to simultaneously take into consideration different phenomena : 1) installation procedure; 2) establishment of equilibrium after installation, and; 3) impact of axial load in the modification of the stress field after installation. For this reason, special attention needs to be taken when in the calculation of β.

A.3.2 End-bearing Capacity

The estimation of end-bearing resistance is given according to API [2011] by :

$$q_p = N_q \times \sigma'_v \tag{A.12}$$

where, N_q is the end bearing factor found in Table 8.

B Broms method for laterally loaded single piles

Broms studied the response of piles in lateral loading for the case of cohesive and cohesionless soils. His analysis is briefly discussed in this section with a focus on the basic ideas of the method, and for a more detailed presentation one may refer to Broms [1964a], Broms [1964b], and Reese et al. [2002].

B.1 Cohesive soil

When in failure of a cohesive soil, the distribution of lateral earth pressure that allows the calculation of lateral capacity is presented in the right of Figure 36. Two important hypothesis are made : 1) the soil situated at $1.5D$ from the surface is not taken into account on calculation, and; 2) the distribution of earth pressure of the soil is approximated from a constant value equal to $9c_uD$, where c_u is the undrained shear strength, and D the diameter of the pile. The first hypothesis is based on the fact that the superficial soil has lower resistance and thus we can imagine a wedge of soil that is moved towards the surface as shown in Figure 36. The second hypothesis, derives from studies on soil movement in both sides of the pile.

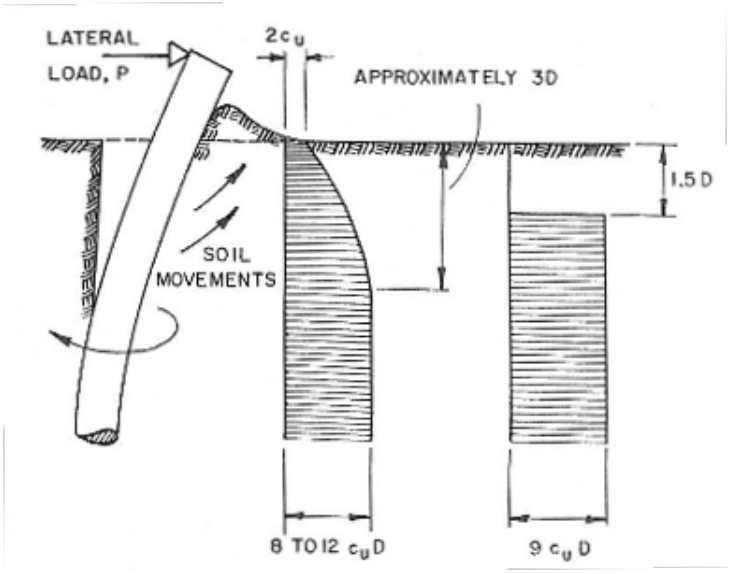

Figure 36: Earth pressure distribution in cohesive soil (Broms [1964a]).

Once the distribution of lateral earth pressure is defined, Broms distinguished separate case studies of failure (Figure 11) and studied the behavior of each case. For example, for a short free-headed pile in cohesive soil, the developing moment of the pile as well as the distribution of earth pressure are represented in Figure 37.

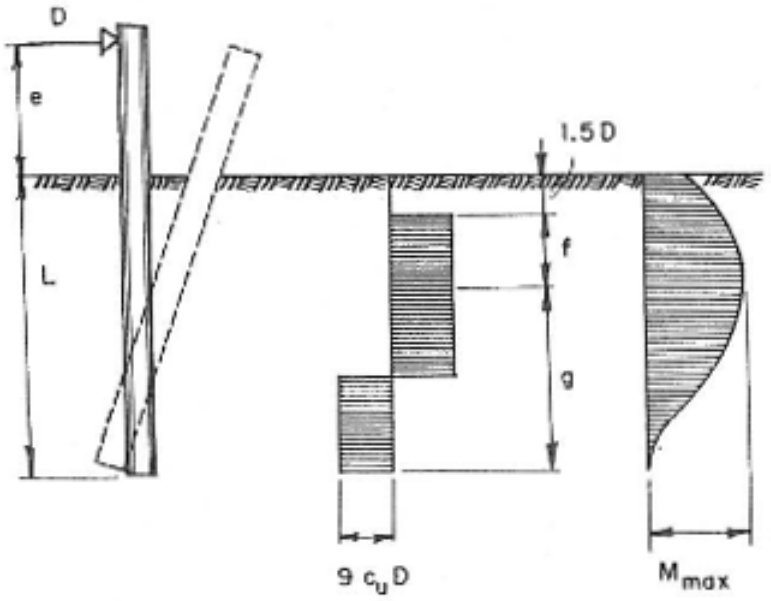

Figure 37: Short pile in cohesive soil : deflection (left), earth pressure (middle), moment(right) (Broms [1964a]).

The expression of maximum moment M_{max}, is given in the section where shear force equals to zero. One can easily define this height from equilibrium:

$$f = \frac{P}{9c_u D} \tag{B.1}$$

Given this value the maximum moment reads :

$$\begin{aligned} M_{max} &= P(e + 1.5D + f) - \frac{9c_u b f^2}{2} \Rightarrow \\ M_{max} &= P(e + 1.5D + 0.5f) \end{aligned} \tag{B.2}$$

The above equation allows the estimation of maximum load P, for which a given moment M_{max} can be supported by the pile-soil system.

When a long pile is considered, we can directly obtain the maximum load P from the equations described above. More precisely, we know that maximum moment M_{max} develops at a distance $1.5D + f$ from the surface. Given the failure mode for long piles (Figure 11b) a plastic hinge develops at the same length and thus the maximum load P is defined directly from equation B.2.

B.2 Cohesionless soil

When in a cohesionless soil, the distribution of earth pressure for a short free-headed pile, is given in Figure 38.

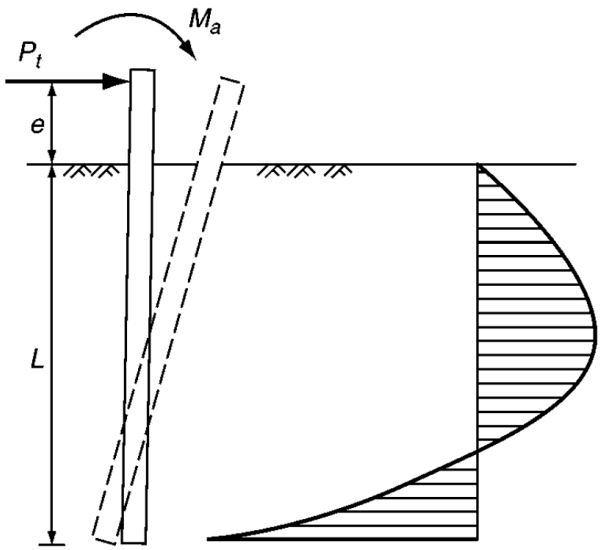

Figure 38: Distribution of earth pressure for short free-headed pile in cohesionless soil (Fleming et al. [2008]).

Broms approximated this distribution of soil, by supposing a triangular one which for the ultimate earth pressure takes a value equal to three times the Rankine passive pressure. In that way, for a given depth z, Broms defines the exerted force as :

$$P_z = 3 \times b \times \gamma \times z \times K_p \tag{B.3}$$

where γ is the unit weight of soil, K_p is coefficient of the passive Rankine earth pressure given by :

$$K_p = \tan^2(45^o + \frac{\phi}{2}) \tag{B.4}$$

After this assumptions he considered the case of Figure 39, supposing an exerted load P_t and a moment M_t in the head.

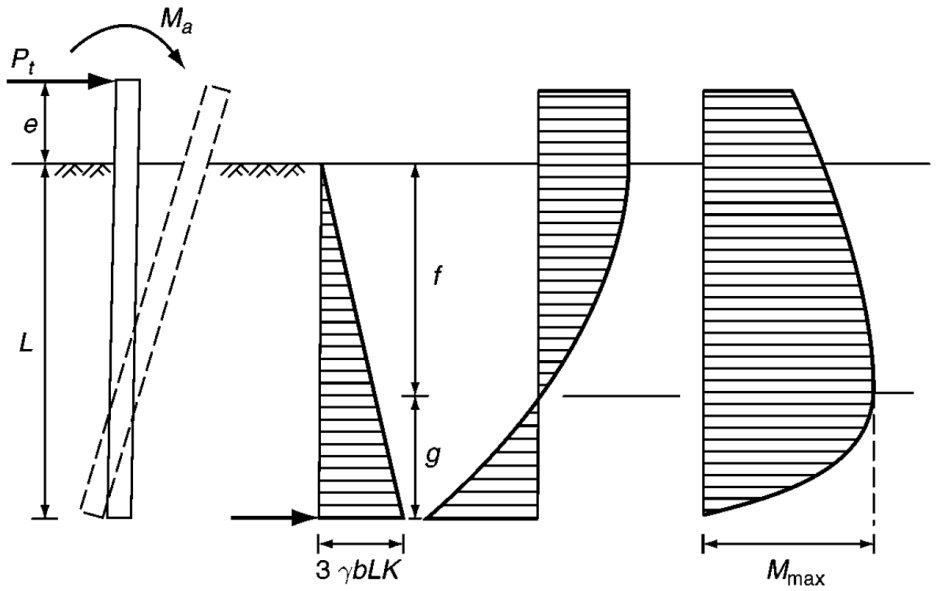

Figure 39: Distribution of deflection, shear, and moment for a short headed pile in cohesionless soil (Fleming et al. [2008]).

The estimation of maximum moment for the pile is given, if an equilibrium is taken at the rotation center. The first step of the analysis is to compute the distance of this rotation center f. An equilibrium of shear stress reads :

$$\begin{aligned} P_t - P_f\frac{f}{2} = P_t - (3b\gamma f K_p)\frac{f}{2} = 0 \Rightarrow \\ f = 0.816\left(\frac{P_t}{\gamma b K_p}\right)^{0.5} \end{aligned} \tag{B.5}$$

The maximum moment can be obtained through the moment equilibrium in the rotation center :

$$M_{max} = P_t(e+f) + M_t - (3b\gamma f K_p)\frac{f}{2}\frac{f}{3} \tag{B.6}$$

Broms repeated equivalent analysis for long piles and medium size piles. Cases with fixed head are also considered and the results are assembled in tables so as to facilitate calculations. Due to page constraints, those tables are not presented here but can be found in Broms [1964a], Broms [1964b], or Reese et al. [2002].